

CANCER

TEAD4 is a master regulator of high-risk nasopharyngeal carcinoma

Ya-Qin Wang^{1†}, Dong-Hong Wu^{1†}, Denghui Wei^{1†}, Jia-Yi Shen^{1†}, Zi-Wei Huang^{1,2†}, Xiao-Yu Liang¹, William C.S. Cho³, Jun Ma¹, Jiawei Lv^{1*}, Yu-Pei Chen^{1*}

The molecular basis underlying nasopharyngeal carcinoma (NPC) remains unclear. Recent progress in transcriptional regulatory network analysis helps identify the master regulator (MR) proteins that transcriptionally define malignant tumor phenotypes. Here, we investigated transcription factor–target interactions and identified TEA domain transcription factor 4 (TEAD4) as an MR of high-risk NPC. Precisely, TEAD4 promoted NPC migration, invasion and cisplatin resistance, depending on its autopalmitylation. Mechanistically, YTHDF2 (YTH domain family 2) recognized WTAP (Wilms tumor 1–associating protein)–mediated TEAD4 m⁶A methylation to facilitate its stability and led to aberrant up-regulation of TEAD4. Up-regulated TEAD4 further drove NPC progression by transcriptionally activating BZW2 (basic leucine zipper and W2 domains 2) to induce the oncogenic AKT pathway. Moreover, the transcriptional activity of TEAD4 was independent of its canonical coactivators YAP/TAZ. Clinically, TEAD4 serves as an independent predictor of unfavorable prognosis and cisplatin response in NPC. Our data revealed the crucial role of TEAD4 in driving tumor malignancy, thus, may provide therapeutic vulnerability in NPC.

INTRODUCTION

Nasopharyngeal carcinoma (NPC) is a metastasis-prone subtype of head and neck cancer with an extremely unbalanced endemic distribution. It is highly prevalent in East Asia and especially common in southern China (1). As per the current guidelines, chemotherapy in combination with radiotherapy is the primary therapeutic method for NPC at high risk of progression (2, 3). Despite recent developments in chemoradiotherapy strategies [e.g., cisplatin-based induction chemotherapy (IC), which reduces distant metastasis] and a better understanding of NPC biology (such as a few genetic changes but frequent epigenetic aberrations), almost all newly diagnosed patients with NPC are empirically treated with intensive cytotoxic chemoradiotherapy, and approximately 20% of them still suffer from distant metastasis (4–6). Thus, further elucidation of the mechanisms underlying NPC progression is required to guide future therapeutic strategies against NPC.

Tumor master regulators (MRs) are transcription factor (TF) proteins that define and regulate the transcriptional identity of a tumor (7). The aberrant activity of MRs is important to maintain the tumor cell state; thus, systematic identification and characterization of tumor MRs will help elucidate the mechanisms responsible for plastic reprogramming across distinct cellular states and provide potential therapeutic vulnerabilities and biomarkers (8–11). Recent developments in systems biology have allowed the interrogation of transcriptional regulatory network models

(interactomes) that, in turn, has opened the way to efficiently identify MR proteins in human malignancies (10–12).

In the present study, we investigated TF–target interactions to decipher the MR protein architecture and identified TEA domain transcription factor 4 (TEAD4) as an MR of NPC at a high risk of progression. Functional assays showed that TEAD4 promoted NPC migration, invasion, and cisplatin resistance, depending on its autopalmitylation. Mechanistically, YTH domain family 2 (YTHDF2) recognized Wilms tumor 1–associating protein (WTAP)–mediated TEAD4 N⁶-methyladenosine (m⁶A) methylation to facilitate its stability and led to the aberrant up-regulation of TEAD4 in NPC. The up-regulated TEAD4 further drove NPC progression by transcriptionally activating the downstream basic leucine zipper and W2 domains 2 (BZW2) to induce the oncogenic AKT signaling pathway. Moreover, the transcriptional activity of TEAD4 was independent of its transcriptional coactivators YAP/TAZ in the canonical Hippo pathway. Last, we elucidated the clinical significance of TEAD4 in patients with NPC. Our study reveals that TEAD4 is an MR protein of high-risk NPC and can act as a potential therapeutic vulnerability for patients with NPC.

RESULTS

TEAD4 is identified as an MR of high-risk NPC

To characterize the MR proteins that regulate the transcriptional state of NPC at high risk of progression, we first applied the Algorithm for the Reconstruction of Accurate Cellular Networks through Adaptive Partitioning (ARACNe-AP) (13) to construct transcriptional interactomes (i.e., TF–target interactions) in gene expression profiles from two public cohorts: cohort 1 comparing NPC samples with or without progression (GSE102349 dataset) and cohort 2 comparing NPC and normal tissue samples (GSE12452 dataset; Fig. 1A). The interactomes of cohort 1 and cohort 2 comprised 65,168 and 200,780 transcriptional interactions, respectively (table S1). We then applied the Virtual Inference of

Copyright © 2023 The Authors, some rights reserved; exclusive licensee American Association for the Advancement of Science. No claim to original U.S. Government Works. Distributed under a Creative Commons Attribution NonCommercial License 4.0 (CC BY-NC).

¹State Key Laboratory of Oncology in South China, Collaborative Innovation Center of Cancer Medicine, Guangdong Key Laboratory of Nasopharyngeal Carcinoma Diagnosis and Therapy, Center for Precision Medicine of Sun Yat-sen University, Sun Yat-sen University Cancer Center, Guangzhou 510060, P.R. China. ²Zhongshan School of Medicine, Sun Yat-sen University, Guangzhou 510060, P.R. China. ³Department of Clinical Oncology, Queen Elizabeth Hospital, Hong Kong Special Administrative Region, Hong Kong, P.R. China.

*Corresponding author. Email: lvjw@sysucc.org.cn (J.-W.L.); chenyp1@sysucc.org.cn (Y.-P.C.)

†These authors contributed equally to this work.

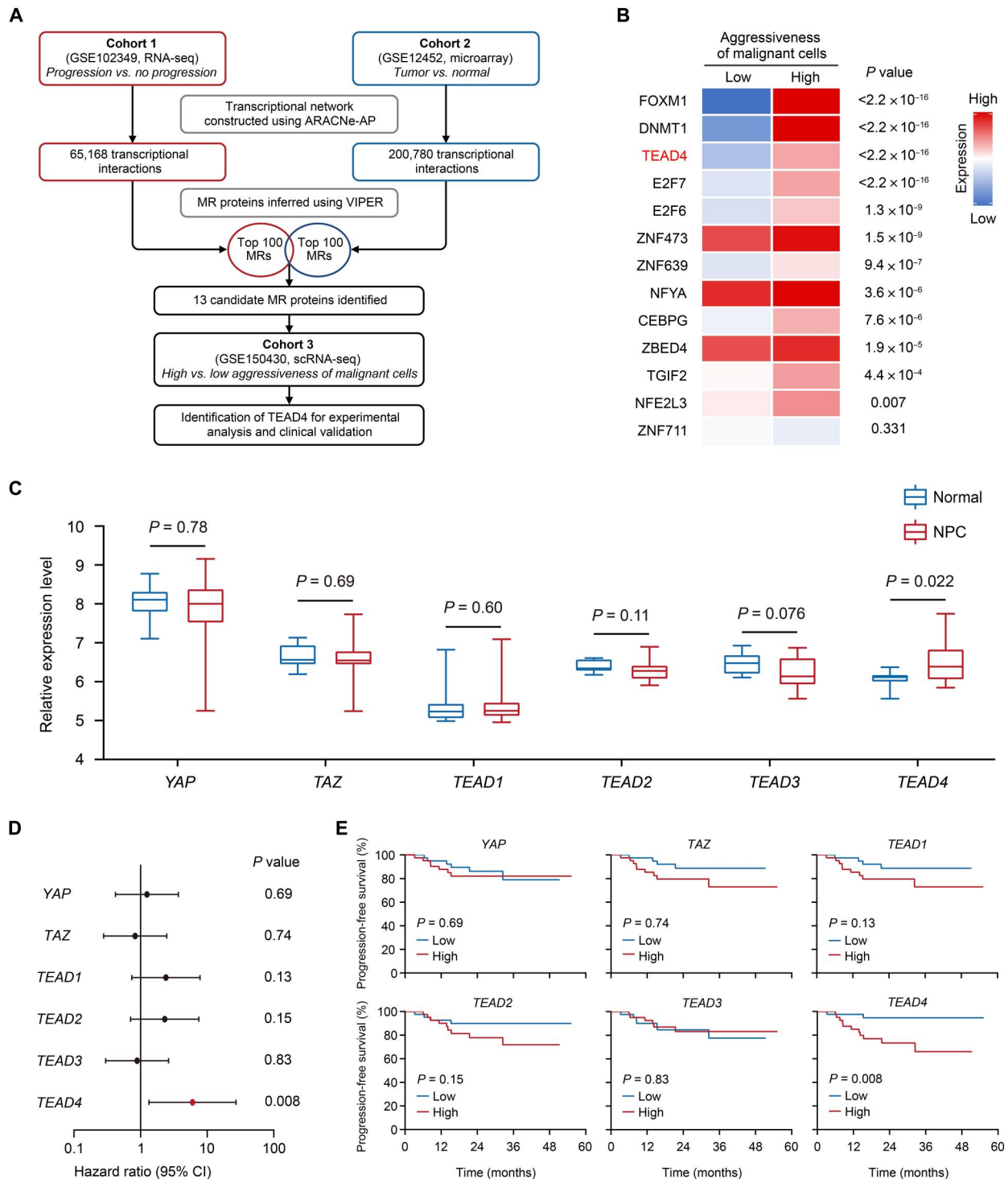


Fig. 1. Identification of TEAD4 as a master regulator of high-risk NPC. (A) The workflow for the inference of MR proteins of NPC at high risk of progression. (B) Heatmap showing the average expression of the 13 candidate MRs in high- and low-aggressiveness groups of malignant cells from cohort 3 (GSE150430 dataset). Division of high- and low-aggressiveness groups according to the median value of scores for a cell cycling signature derived from our previous study of 5397 malignant cells profiled by scRNA-seq. P values were calculated using Wilcoxon rank sum test. (C) Box plots depicting the expression of YAP, TAZ, and TEAD1 to TEAD4 from the Hippo signaling pathway in NPC ($n = 31$) versus normal ($n = 10$) tissue samples from the GSE12452 dataset, showing a significant difference only for TEAD4. The box plot center corresponds to the median, the upper and lower lines of the box correspond to the interquartile range, and the whiskers correspond to the 1.5 \times interquartile range. P values were calculated using Wilcoxon rank sum test. (D and E) Forest plot (D) and Kaplan-Meier curves (E) showing associations of the expression levels of YAP, TAZ, and TEAD1 to TEAD4 with the progression-free survival of 82 patients from the GSE102349 dataset. A significant association was shown only for TEAD4. The expression of YAP, TAZ, and TEAD1 to TEAD4 was divided into high and low groups according to their median values, respectively. P values in (D) and (E) were calculated using a log-rank test.

Protein Activity by Enriched Regulon (VIPER) algorithm (10, 11) to prioritize MR proteins in certain disease states (i.e., progression versus nonprogression in cohort 1, and tumor versus normal in cohort 2) based on the inferred transcriptional activity. Overlapping the top-ranking 100 MRs from each cohort (table S2), we identified 13 candidate MRs of high-risk NPC (fig. S1).

Next, we assessed the association of the 13 candidate MRs with the aggressiveness of NPC malignant cells using the single-cell RNA sequencing (scRNA-seq) cohort from our recent study (GSE150430 dataset) (14). For each malignant cell, we calculated the score of the cell cycling signature, which was derived from our scRNA-seq study and could reflect cellular aggressiveness (14). Notably, the expression of four MRs showed the most significant enrichment in highly aggressive malignant cells: FOXM1, DNMT1, TEAD4, and E2F7 (Fig. 1B). Among these four MRs, FOXM1, DNMT1, and the E2F family have already been well characterized in NPC tumorigenesis in our previous studies and others (15–17), while the role of TEAD4 in NPC remains unknown.

TEAD4 belongs to the TEAD protein family. TEADs are activated by their canonical cotranscriptional effectors (i.e., YAP and TAZ) in the Hippo signaling pathway and have been implicated in the regulation of tissue growth and cell fate (18, 19). Evaluating the expression of *YAP*, *TAZ*, and *TEAD1* to *TEAD4* in NPC versus normal tissue samples in the GSE12452 dataset revealed that only *TEAD4* was significantly up-regulated in NPC (Fig. 1C). In addition, higher expression of *TEAD4* was significantly associated with an increased risk of disease progression in patients with NPC (GSE102349 dataset), whereas no significant differences were observed for other genes (Fig. 1, D and E). Collectively, these data indicated that TEAD4 might play an important role in NPC progression.

TEAD4 promotes NPC migration, invasion, and cisplatin resistance in vitro

Consistent with the above findings, we found that TEAD4 was markedly up-regulated in NPC compared with normal nasopharyngeal tissues at both the mRNA and protein levels (Fig. 2, A and B). In line with the patient data, the expression of TEAD4 was significantly higher in NPC cell lines than in normal nasopharyngeal epithelial cell lines (NP69 and N2-Tert; Fig. 2C). To gain further insight into the function of TEAD4 in NPC, we performed gene set enrichment analysis (GSEA) based on NPC gene expression profiles in the GSE102349 dataset and found significant enrichment of gene sets related to metastasis and cisplatin resistance in the high *TEAD4* expression group (Fig. 2D). To further investigate the effect of TEAD4 on NPC cell phenotypes, we generated SUNE-1 and HONE-1 cells with stable knockdown or TEAD4 overexpression (fig. S2, A to D). Transwell migration, invasion, and wound healing assays demonstrated that TEAD4 knockdown markedly impaired the migratory and invasive abilities of NPC cells (Fig. 2, E and F, and fig. S2E). We further determined that the migratory and invasive abilities of NPC cells were substantially enhanced by exogenous overexpression of TEAD4 (fig. S2, F to H). In addition, TEAD4 knockdown also inhibited NPC cell proliferation (fig. S3). To assess the effect of TEAD4 on cisplatin sensitivity, we performed Cell Counting Kit-8 (CCK-8) and cell apoptosis assays and found significantly increased sensitivity of NPC cells to cisplatin after TEAD4 knockdown (Fig. 2G and fig. S4, A to C). The opposite was observed when TEAD4 was overexpressed exogenously (fig. S4, D to G). In contrast to TEAD4, other TEAD members

(TEAD1 to TEAD3) only showed weak or marginal effects on NPC cell migration and cisplatin resistance (fig. S5).

As autopalmitoylation is reported to be important for the function of TEAD4 (20–22), we further investigated whether TEAD4 autopalmitoylation affects its function in NPC. We adopted MGH-CPI, an inhibitor that could bind to the palmitoylation pocket of TEAD4 (22), to reduce the palmitoylation level of TEAD4 (Fig. 2H) and found that the migration, invasion, and cisplatin resistance of NPC cells were significantly inhibited (Fig. 2, I and J, and fig. S6, A and B). In addition, restoring the expression of palmitoylation-deficient TEAD4 mutants, TEAD4^{C335S} and TEAD4^{C367A} (fig. S6C) (21), did not reverse the inhibitory effect of TEAD4 knockdown on NPC cell migration, invasion, and cisplatin resistance (fig. S6, D and E). Overall, these results indicate that TEAD4 promotes NPC migration, invasion, and cisplatin resistance, dependent on its autopalmitoylation.

TEAD4 mRNA is stabilized by YTHDF2 via WTAP-mediated m⁶A modification in NPC

We then probed the mechanism underlying the aberrant up-regulation of TEAD4 in NPC. First, we analyzed the mutation and copy number variation data of NPC in the GSE102349 dataset and found low mutation (0.9%) and amplification (8.1%) frequencies of *TEAD4* (fig. S7A). The DNA methylation levels of *TEAD4* in our previously published study (GSE52068 dataset) were also examined (23), and no significant differences were observed between the normal nasopharynx and NPC tissues (fig. S7B). Next, we investigated whether m⁶A RNA modification, the most abundant epigenetic modification in eukaryotic mRNA (24), might be involved. Using the online prediction tool SRAMP (25) that predicted m⁶A sites along the *TEAD4* sequence, we found strong m⁶A peak enrichment of *TEAD4*, in which three m⁶A sites (RRACH motifs) at 791 to 1104 nt (exon 9/10 of 13) were predicted with a high confidence threshold (Fig. 3, A and B). We further performed methylated RNA immunoprecipitation (MeRIP)-quantitative polymerase chain reaction (qPCR) assays in NP69, SUNE-1, and HONE-1 cells and found that the m⁶A levels of *TEAD4* were significantly higher in NPC cells than in normal nasopharyngeal epithelial cells (Fig. 3C), suggesting a role for m⁶A modification in the regulation of TEAD4 expression.

To further identify the specific m⁶A regulators, we examined the correlations between the RNA levels of common m⁶A regulators and *TEAD4* in the GSE102349 dataset and found that the expression of members from two reader families, insulin-like growth factor 2 mRNA-binding protein family (IGF2BP1 to IGF2BP3) and YTHDF1 and YTHDF2, demonstrated prominent correlations with *TEAD4* expression (Fig. 3D). We then constructed small interfering RNAs targeting the IGF2BP and YTHDF reader families and found that YTHDF2 knockdown markedly decreased the expression of *TEAD4*, and the effect was more prominent than that in other IGF2BP and YTHDF family members (fig. S8). We further confirmed that protein levels of TEAD4 were decreased by YTHDF2 knockdown in SUNE-1 and HONE-1 cells (Fig. 3E). These data suggested that the expression of TEAD4 was regulated by YTHDF2 in NPC cells. The function of YTHDF2 as an m⁶A reader is to destabilize m⁶A-tagged transcripts by activating mRNA degradation pathways (26–28). However, its role in NPC remains unclear. Comparing NPC and normal tissue samples from the GSE12452 dataset, we found a significant up-regulation

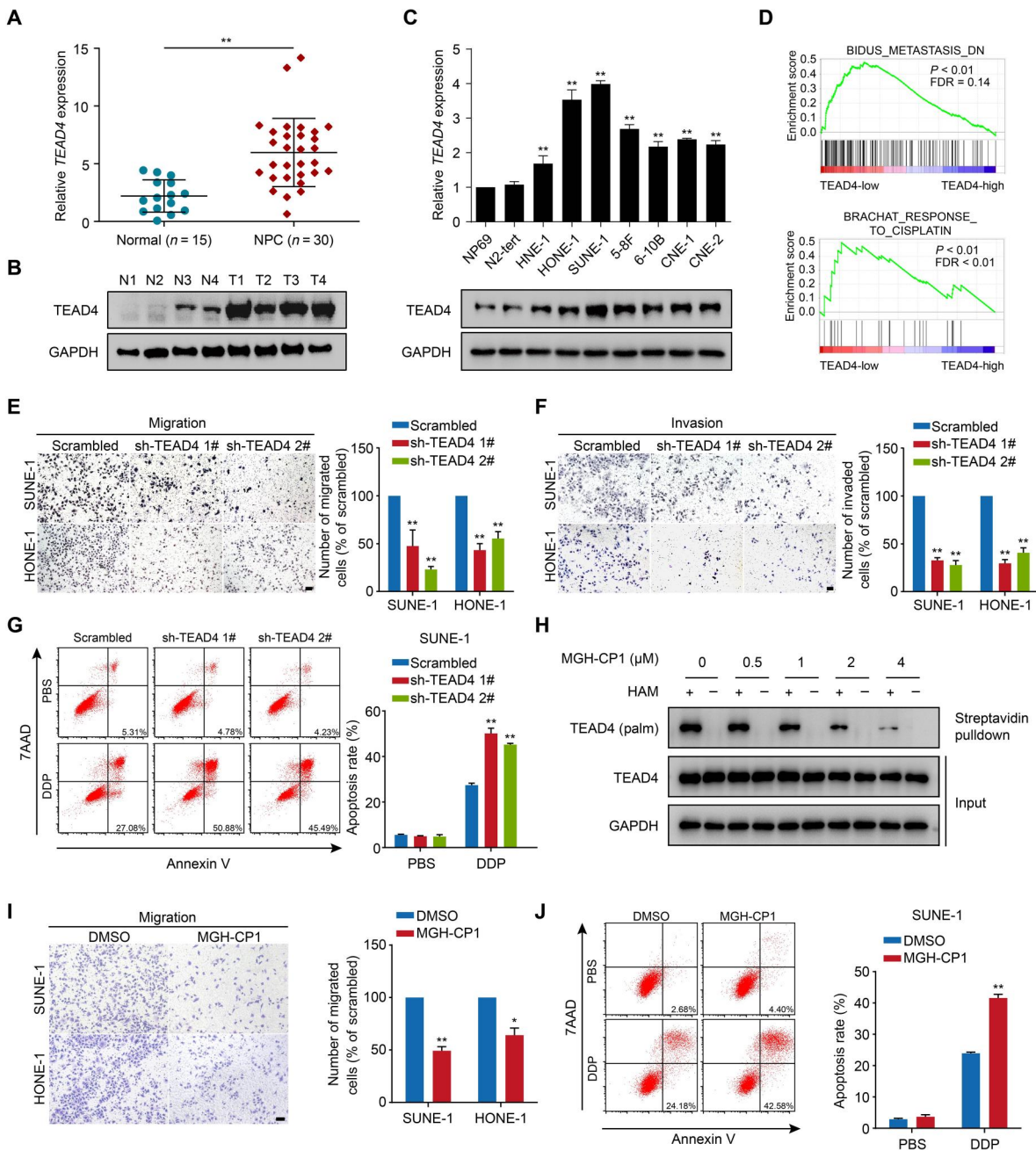


Fig. 2. TEAD4 promotes migration, invasion, and cisplatin resistance of NPC cells in vitro. (A) Quantitative real-time polymerase chain reaction (qRT-PCR) analysis of *TEAD4* expression in normal nasopharynx tissues and NPC. (B) Western blot analysis of *TEAD4* expression in normal nasopharynx and NPC tissues (N, normal; T, tumor). GAPDH, glyceraldehyde-3-phosphate dehydrogenase. (C) qRT-PCR (top) and Western blot (bottom) analyses of *TEAD4* expression in normal nasopharyngeal epithelial and NPC cell lines. (D) GSEA of gene sets related to metastasis and cisplatin resistance in the high *TEAD4* expression group in the GSE102349 dataset. (E and F) Representative images (left) and quantification of migratory or invasive cells (right) of Transwell migration (E) and invasion (F) assays in SUNE-1 and HONE-1 cells with or without *TEAD4* knockdown. Scale bar, 100 μ m. (G) Representative images (left) and apoptosis rate (right) of cell apoptosis assays in SUNE-1 cells exposed to phosphate-buffered saline (PBS) or cisplatin (DDP), with or without *TEAD4* knockdown. (H) Streptavidin blot detection of palmitoylated *TEAD4* in SUNE-1 cells exposed to the indicated doses of MGH-CP1 for 24 hours by acyl-biotin exchange assay with or without hydroxylamine (HAM; 1 M). (I) Representative images (left) and quantification of migratory cells (right) of Transwell migration assays in SUNE-1 and HONE-1 cells exposed to dimethyl sulfoxide (DMSO) or MGH-CP1 (2 μ M, 24 hours). Scale bar, 100 μ m. (J) Representative images (left) and apoptosis rate (right) of cell apoptosis assays in SUNE-1 cells exposed to PBS or DDP, with or without MGH-CP1 (2 μ M, 24 hours) treatment. Data in (A), (C), (E) to (G), (I), and (J) are presented as means \pm SD; $n = 3$ independent experiments (C, E to G, I, and J). P values were calculated using unpaired Student's t test (A, I, and J) or one-way analysis of variance (ANOVA; C and E to G). * $P < 0.05$ and ** $P < 0.01$.

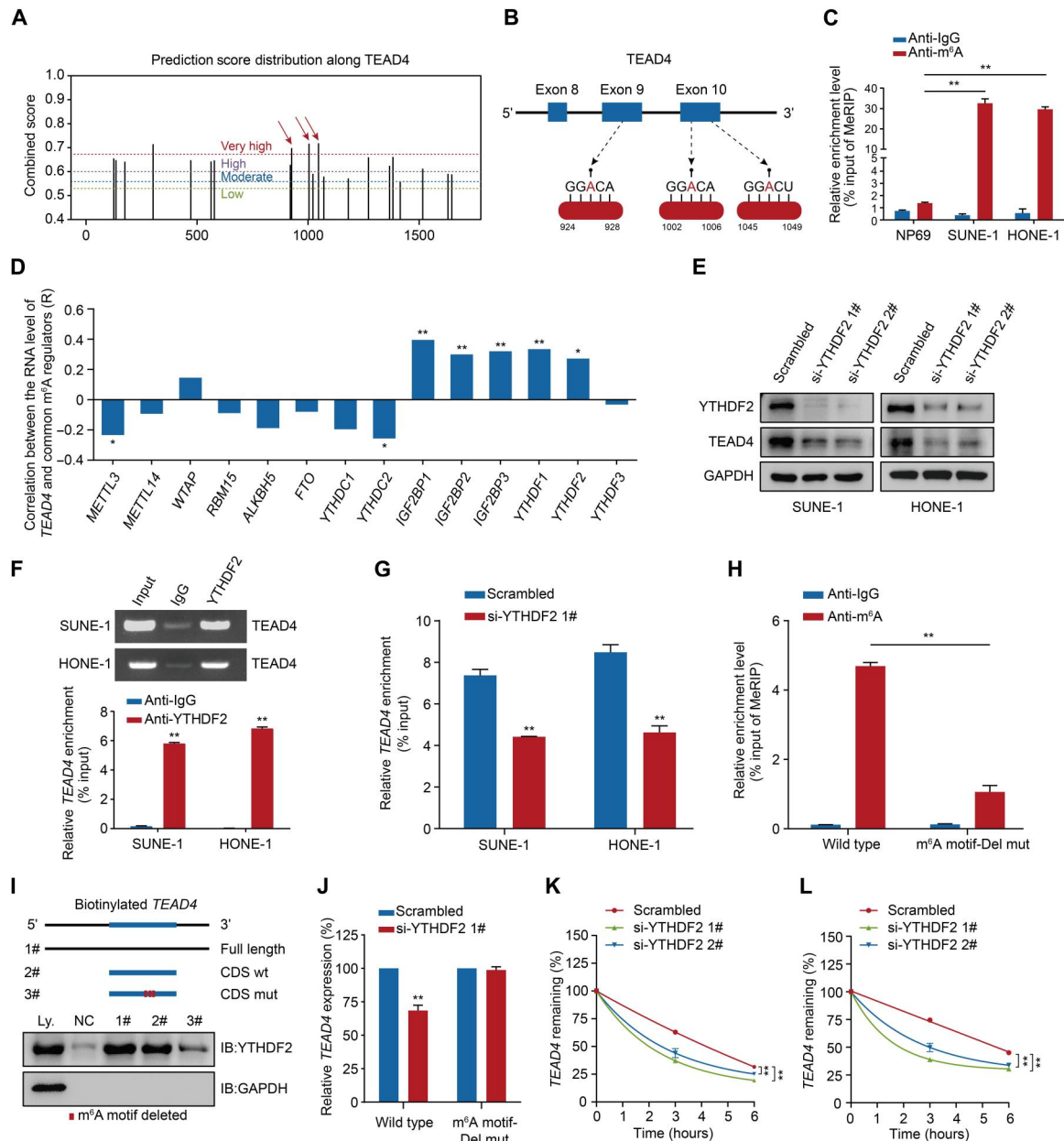


Fig. 3. TEAD4 expression in NPC cells is up-regulated in an m⁶A-dependent manner. (A) Enriched and specific m⁶A peak distribution of *TEAD4* transcripts predicted by SRAMP. (B) Diagram depicting the position of m⁶A motifs with a high combined score predicted by SRAMP within *TEAD4* transcripts. (C) MeRIP-qPCR assays showing the m⁶A levels of *TEAD4* transcripts in normal nasopharyngeal epithelial and NPC cells. (D) Pearson's correlations between the mRNA expression of common m⁶A regulators and *TEAD4* in the GSE102349 dataset. (E) Western blot analysis of *TEAD4* expression in SUNE-1 and HONE-1 cells with or without YTHDF2 silencing. (F) Agarose electrophoresis (top) and qRT-PCR (bottom) analysis of RIP assays showing YTHDF2 occupation in *TEAD4* in SUNE-1 and HONE-1 cells. (G) RIP-qPCR analysis of YTHDF2 occupation in *TEAD4* in SUNE-1 and HONE-1 cells with or without YTHDF2 silencing. (H) MeRIP-qPCR assays to analyze the m⁶A levels of *TEAD4* in SUNE-1 cells transfected with *TEAD4* wild-type or its m⁶A motif depletion mutant construct. (I) Western blot analysis of YTHDF2 expression after RNA pull-down assay with cell lysate (Ly.), beads only (NC), full-length biotinylated-*TEAD4*, and coding DNA sequence (CDS) region of *TEAD4* without or with m⁶A motif depletion in SUNE-1 cells. (J) qRT-PCR analysis of *TEAD4* expression in SUNE-1 cells transfected with *TEAD4* wild-type or mutant construct together with YTHDF2 small interfering RNAs or its scramble. (K and L) Decay rate of mRNA and qRT-PCR analysis of *TEAD4* at different time points after actinomycin D (5 μg/ml) treatment in SUNE-1 (K) and HONE-1 (L) cells with or without YTHDF2 silencing. Data in (C), (F) to (H), (J), (K), and (L) are presented as means ± SD; n = 3 independent experiments. P values were calculated using one-way ANOVA (C, K, and L), Pearson correlation test (D), or unpaired Student's t test (F to H and J). *P < 0.05 and **P < 0.01.

of *YTHDF2* in NPC (fig. S9A), which echoed the high expression of *TEAD4* in NPC tumor tissues. We then performed an RIP assay and identified direct physical interactions between *TEAD4* mRNA and *YTHDF2* (Fig. 3F). Moreover, the enrichment levels of *TEAD4* mRNA decreased after *YTHDF2* inhibition (Fig. 3G). Consistently, the RNA pull-down assay demonstrated that *YTHDF2* bound *TEAD4* full-length transcripts in SUNE-1 and HONE-1 cells (fig. S9B). To further confirm whether *YTHDF2* up-regulated *TEAD4* expression in an m⁶A-dependent manner, we constructed plasmids encoding the mutant *TEAD4* coding DNA sequence (CDS) in which the m⁶A motifs were deleted. MeRIP-qPCR showed an apparent decrease in m⁶A levels in *TEAD4* mutant transcripts compared with the wild type, indicating that the m⁶A motifs within 791 to 1104 nt of *TEAD4* were responsible for its m⁶A modification (Fig. 3H). RNA pull-down assay revealed that the binding of *YTHDF2* to *TEAD4* transcripts was specifically impaired by m⁶A motif depletion (Fig. 3I). Moreover, silencing *YTHDF2* significantly decreased the expression of *TEAD4* in the wild type but not in the mutant transcripts (Fig. 3J). Actinomycin D chase experiments also confirmed the decreased RNA stability of *TEAD4* after *YTHDF2* silencing in NPC cells (Fig. 3, K and L).

We next explored the methyltransferase involved in enhancing *TEAD4* m⁶A modification. As shown in Fig. 3D, a positive correlation was observed between the expression of *TEAD4* and *WTAP*, an m⁶A methyltransferase reported to promote NPC progression (29). We further confirmed that *TEAD4* expression was significantly reduced at the mRNA and protein levels after *WTAP* silencing in NPC cells (fig. S9, C to E). MeRIP-qPCR and actinomycin D chase experiments showed significantly decreased m⁶A levels and RNA stability of *TEAD4* after *WTAP* inhibition (fig. S9, F to H). Furthermore, the RIP assay demonstrated that *WTAP* silencing markedly impaired the binding of *YTHDF2* to *TEAD4* transcripts (fig. S9I). Collectively, these data indicate that *YTHDF2* recognizes *WTAP*-mediated *TEAD4* m⁶A methylation to enhance the stability and up-regulation of *TEAD4* in NPC.

TEAD4 drives NPC progression via BZW2 transcription activation to induce the AKT pathway

Next, we elucidated the underlying mechanism of *TEAD4*-driven malignant phenotypes in NPC by performing chromatin immunoprecipitation sequencing (ChIP-seq) using HONE-1 cells overexpressing *TEAD4* (table S3). By overlapping the ChIP-seq data with genes displaying significant correlations with *TEAD4* levels ($R > 0.4$ and $P < 0.05$) in the GSE12452 and GSE102349 datasets, we identified 10 potential direct targets of *TEAD4* (Fig. 4A). Subsequent quantitative real-time PCR (qRT-PCR) analysis revealed that the expression of *BZW2*, *LARP6*, and *RCSD1* was significantly increased or decreased after overexpression or knockdown of *TEAD4*, respectively; among these, *BZW2* demonstrated the most prominent change (Fig. 4B and fig. S10, A and B). We further confirmed that *TEAD4* expression change had the most evident effect on the protein levels of *BZW2*, compared with *LARP6* or *RCSD1* (Fig. 4, C and D). This linkage change of *BZW2* and *TEAD4* was also recapitulated in other human NPC cell lines (5-8F, 6-10B, and HNE-1; fig. S10, C to F). In addition, correlative expression patterns of *TEAD4* and *BZW2* were observed across multiple human cancer cell lines, including SUNE-1 and HONE-1 (NPC), A549 (lung adenocarcinoma), HeLa (cervical cancer), SW620 (colorectal cancer), MDA-MB-231 (breast cancer), T24 (bladder cancer), and HepG2

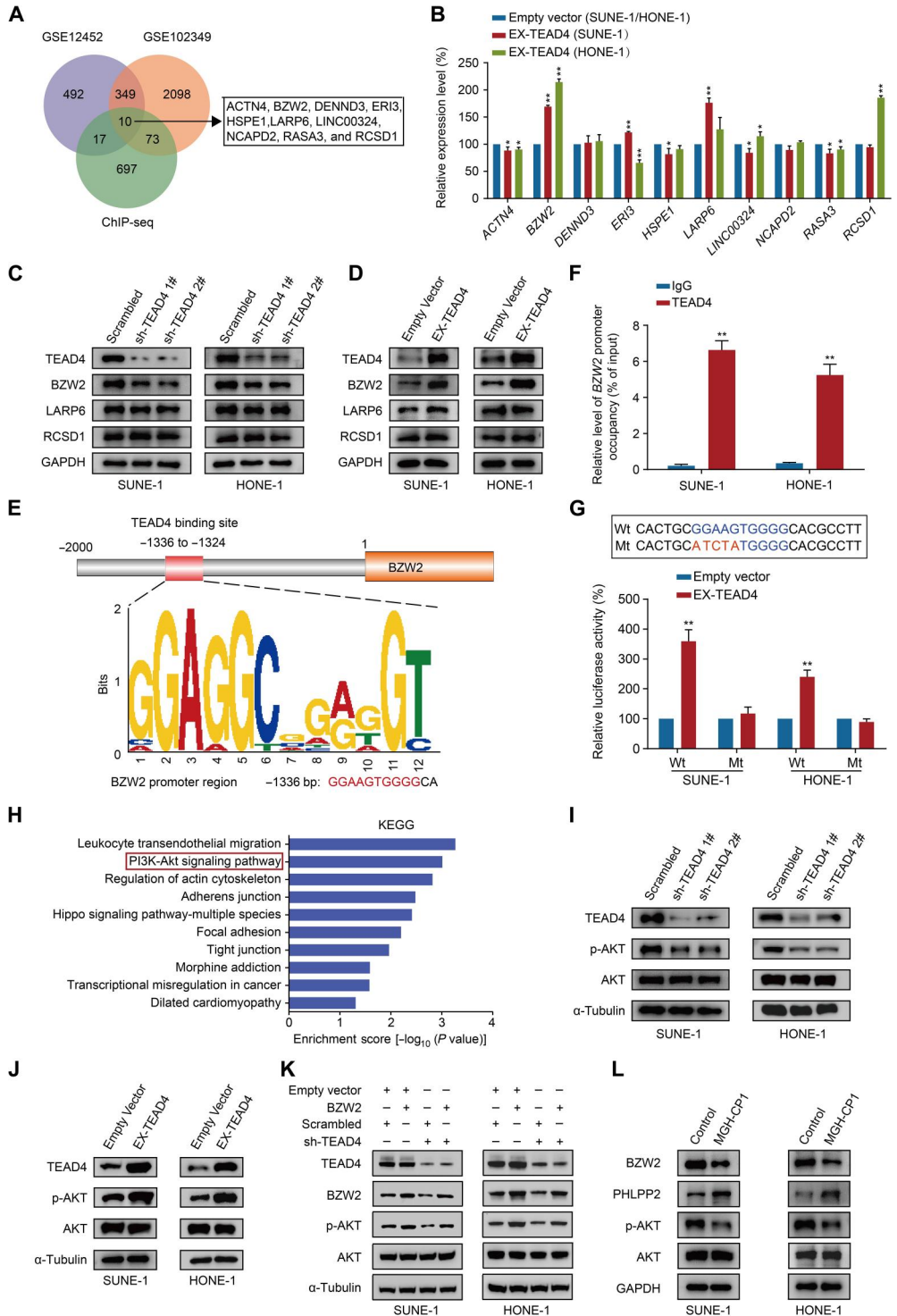
(hepatocellular carcinoma) cells (fig. S10, G and H). Collectively, these data suggest that *BZW2* is a strong *TEAD4* target.

BZW2 belongs to the basic leucine zipper (bZIP) superfamily of TFs, and its function is yet to be fully described. In NPC, we found a significant up-regulation of *BZW2* in tumors compared with normal tissue samples (fig. S11A), and *BZW2* knockdown markedly inhibited the migration, invasion, and cisplatin resistance of NPC cells (fig. S11, B to F). To further address the role of *BZW2* as the downstream target of *TEAD4*, we first predicted one cis-element for *TEAD4* located within -1336 to -1324 base pairs (bp) upstream of the *BZW2* transcriptional start site based on ChIP-seq data (Fig. 4E). ChIP-qPCR assays verified the binding of *TEAD4* to the *BZW2* promoter in multiple NPC cell lines (Fig. 4F and fig. S12A). In line with the above findings (Fig. 4, B to D, and fig. S10, A and B), the enrichment of *TEAD4* in the promoter regions of *LARP6* and *RCSD1* was not evident (fig. S12, B and C). Furthermore, we performed luciferase reporter assays and found that overexpression of *TEAD4* significantly increased the luciferase activity of the wild-type *BZW2* promoter construct, and mutations in the cis-element substantially abolished promoter activity (Fig. 4G), confirming that *TEAD4* directly binds to the promoter of *BZW2* to drive its transcription. Last, to determine whether *TEAD4* promoted NPC progression by up-regulating *BZW2*, we performed in vitro functional rescue assays by restoring the expression of *BZW2* in *TEAD4*-knockdown cells and found that the inhibitory effect of *TEAD4* knockdown on NPC cell migration, invasion, and cisplatin resistance was significantly reversed by *BZW2* overexpression (fig. S13). Overall, these findings demonstrate that *TEAD4* transcriptionally activates *BZW2* to drive malignant phenotypes in NPC.

To understand the biological pathways underlying the *TEAD4*-*BZW2* axis in NPC progression, we performed a Kyoto Encyclopedia of Genes and Genomes pathway analysis based on *TEAD4* target genes from our ChIP-seq data (table S3) and identified AKT signaling, an important pathway in tumorigenesis (30), as one of the most enriched pathways (Fig. 4H). Western blot assays confirmed that phospho-AKT (p-AKT) expression was significantly reduced or enhanced in *TEAD4*-knockdown or *TEAD4*-overexpressed NPC cells, respectively (Fig. 4, I and J). Furthermore, GSEA results revealed that low *BZW2* expression was negatively correlated with AKT signaling (fig. S14A), as confirmed by Western blot analysis (fig. S14B). Consistently, *BZW2* overexpression rescued the inhibition of p-AKT induced by *TEAD4* knockdown (Fig. 4K). We then analyzed the public ChIP-seq data for *BZW2* (GSE174559) (31) to explore how *BZW2* activates AKT signaling. In silico analysis revealed several potential *BZW2* transcriptional target genes that also act as upstream regulators of AKT signaling, among which the expression of PH domain and leucine-rich repeat protein phosphatase 2 (*PHLPP2*), a well-documented AKT phosphatase that inactivates AKT (32, 33), was significantly increased after *BZW2* knockdown in NPC cells (fig. S14, C and D). This negative association was also confirmed at the protein level (fig. S14E). ChIP-qPCR and luciferase reporter assays revealed that *PHLPP2* was transcriptionally repressed by *BZW2* (fig. S14, F and G), and silencing of *PHLPP2* rescued the inhibitory effect of *BZW2* knockdown on p-AKT (fig. S14H). Moreover, MGH-CP1 significantly impaired *BZW2* expression and AKT activation while promoting *PHLPP2* expression in NPC cells (Fig. 4L). Collectively, these results indicate that *TEAD4* promotes *BZW2* transcription to activate the AKT pathway in NPC cells.

Fig. 4. TEAD4 activates *BZW2* transcription to induce the AKT pathway.

(A) Identification of potential targets of TEAD4. Ten genes were identified by overlapping the genes with significant correlations with *TEAD4* levels (Pearson $R > 0.4$, $P < 0.05$) in the GSE12452 and GSE102349 datasets, and the TEAD4 target genes from ChIP-seq data (table S3). **(B)** qRT-PCR analysis of the expression of the 10 genes [in (A)] in SUNE-1 and HONE-1 cells with or without TEAD4 overexpression. **(C and D)** Western blot analysis of *BZW2*, *LARP6*, and *RCSD1* expression after TEAD4 knockdown (C) or overexpression (D) in SUNE-1 and HONE-1 cells. **(E)** Schema of the putative TEAD4-binding site in the promoter region of *BZW2*. Comparisons of the TEAD4-binding sequences (predicted by ChIP-seq analysis) and promoter region of the *BZW2* are shown in the bottom panel. **(F)** ChIP-qPCR analysis of endogenous TEAD4 occupation on the binding site of *BZW2* promoter in SUNE-1 and HONE-1 cells. **(G)** Luciferase reporter assays of *BZW2* activity in SUNE1 and HONE1 cells transfected with plasmids encoding control vector or TEAD4 together with *BZW2* promoter wild-type or mutant constructs. **(H)** Kyoto Encyclopedia of Genes and Genomes analysis based on TEAD4 target genes identified by ChIP-seq assay (table S3). **(I and J)** Western blot analysis of AKT activation after TEAD4 knockdown (I) or overexpression (J) in SUNE-1 and HONE-1 cells. **(K)** Western blot analysis showing the effect of *BZW2* overexpression on AKT activation in SUNE-1 and HONE-1 cells with or without TEAD4 knockdown. **(L)** Western blot analysis of *BZW2*, *PHLPP2*, phospho-AKT (p-AKT), and AKT in SUNE-1 and HONE-1 cells exposed to DMSO or MGH-CP1 (2 μ M, 24 hours). Data in (B), (F), and (G) are presented as means \pm SD; $n = 3$ independent experiments. P values were calculated using unpaired Student's t test. * $P < 0.05$ and ** $P < 0.01$.



TEAD4 promotes NPC migration, invasion, and cisplatin resistance independent of YAP/TAZ modulation

YAP and TAZ are canonical transcriptional coactivators of TEAD4 in the Hippo signaling pathway (18). Therefore, we investigated whether YAP/TAZ was required for TEAD4-driven NPC progression. Western blot assays showed that YAP or TAZ silencing in NPC cells did not affect the expression of TEAD4 (fig. S15, A and B), and

TEAD4 knockdown did not affect YAP or TAZ expression (fig. S15C). We then performed coimmunoprecipitation (co-IP) assays and found that the endogenous interaction between TEAD4 and YAP/TAZ was weak in NPC cells (Fig. 5A), compared with breast cancer or bladder cancer cells, in which the YAP/TAZ-TEAD4 complex has been reported to drive malignant phenotypes (fig. S16, A and B) (34, 35). Furthermore, we performed gel filtration

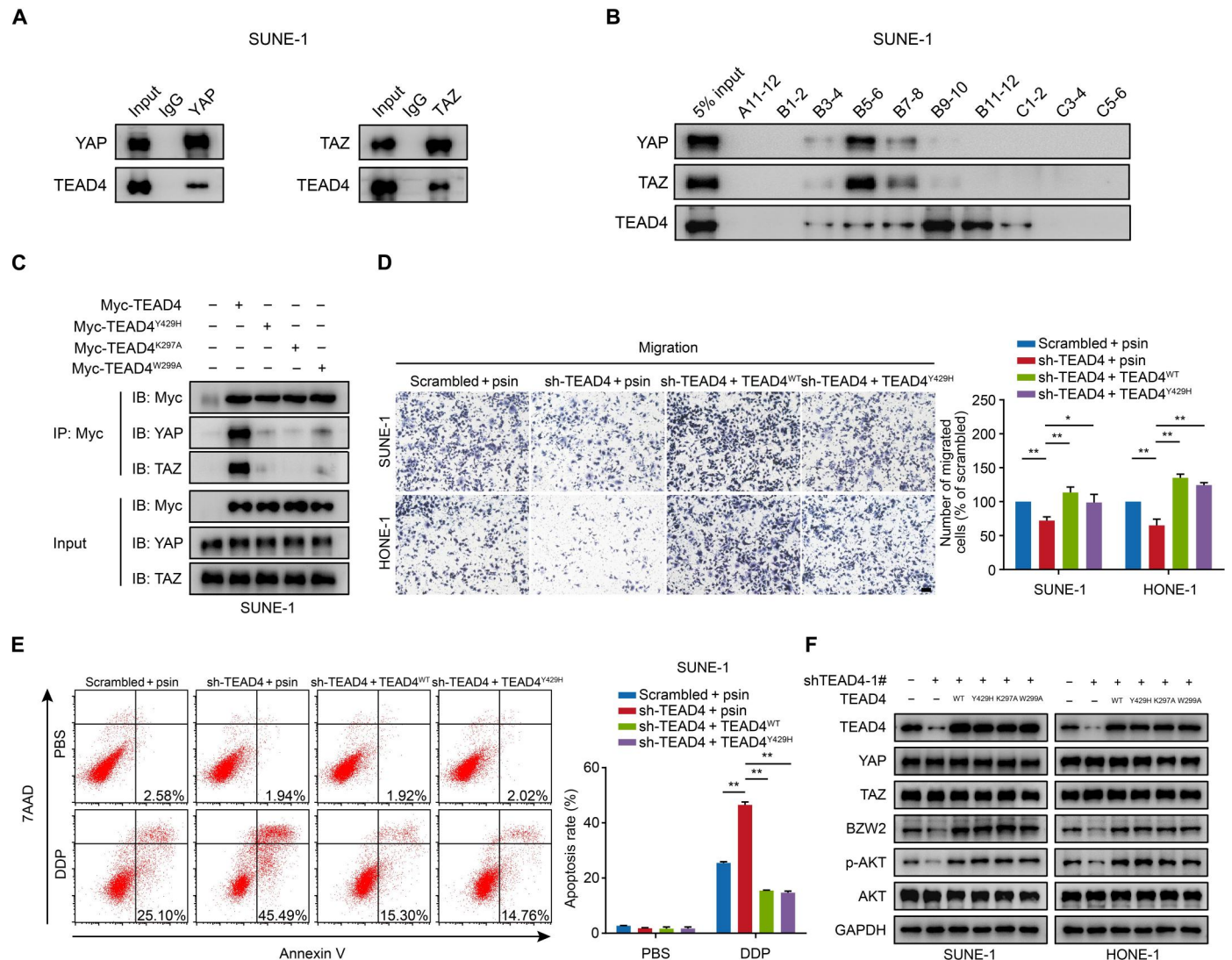


Fig. 5. TEAD4 promotes NPC metastasis and chemoresistance independent of YAP/TAZ modulation. (A) Lysates from SUNE-1 cells were immunoprecipitated with anti-YAP or anti-TAZ antibodies and subjected to Western blot analysis with anti-TEAD4 and anti-YAP or anti-TAZ antibodies. (B) Gel filtration chromatography analysis of SUNE-1 cell lysates. Forty-eight fractions (A1 to A12, B1 to B12, C1 to C12, and D1 to D12) were collected and the A11 to C6 fractions were shown; proteins pooled from two fractions were run on each lane. (C) Lysates from SUNE-1 cells transfected with Myc-TEAD4^{WT}, Myc-TEAD4^{Y429H}, Myc-TEAD4^{K297A}, or Myc-TEAD4^{W299A} were immunoprecipitated with an anti-Myc antibody and subjected to Western blot analysis with the anti-Myc, anti-YAP, or anti-TAZ antibodies. (D) Representative images (left) and quantification of migratory cells (right) of Transwell migration assays in TEAD4-knockdown SUNE-1 and HONE-1 cells transfected with plasmids encoding TEAD4^{WT} or TEAD4^{Y429H}. Scale bar, 100 μ m. (E) Representative images (left) and apoptosis rate (right) of cell apoptosis assays in TEAD4-knockdown SUNE-1 cells transfected with plasmids encoding TEAD4^{WT} or TEAD4^{Y429H} and exposed to PBS or cisplatin (DDP). (F) Western blot analysis of TEAD4, YAP/TAZ, BZW2, p-AKT, and AKT in TEAD4-knockdown SUNE-1 and HONE-1 cells transfected with plasmids encoding TEAD4^{WT}, TEAD4^{Y429H}, TEAD4^{K297A}, or TEAD4^{W299A}. Data in (D) and (E) are presented as means \pm SD; $n = 3$ independent experiments. P values were calculated using one-way ANOVA. * $P < 0.05$ and ** $P < 0.01$.

chromatography analysis and found that low levels of TEAD4 formed complexes with YAP/TAZ in NPC (Fig. 5B). In contrast, TEAD4 was found to be largely comigrated in the same fractions as YAP/TAZ in breast cancer and bladder cancer cells (fig. S16, C and D). These results prompted us to presume that the function of TEAD4 may be independent of YAP/TAZ modulation in NPC. To address this, we constructed plasmids encoding YAP/TAZ binding-deficient TEAD4 mutants, TEAD4^{Y429H}, TEAD4^{K297A}, and TEAD4^{W299A} (Fig. 5C) (21, 36, 37), and found that restoring the expression of both TEAD4^{WT} and YAP/TAZ binding-deficient

mutant TEAD4 efficiently rescued the impaired abilities of NPC cell migration, invasion, and cisplatin resistance in TEAD4-knockdown NPC cells (Fig. 5, D and E, and fig. S17). In addition, downstream BZW2 expression and AKT activation were rescued after the restoration of the TEAD4 mutants (Fig. 5F). Consistently, in YAP/TAZ double-knockout NPC cells, restoring TEAD4 expression significantly reversed the inhibitory effect of TEAD4 knockdown on NPC migration, invasion, and cisplatin resistance, as well as BZW2 expression and AKT activation (fig. S18). Together, our

data indicate that TEAD4 promotes NPC progression in a YAP/TAZ-independent manner.

TEAD4 promotes NPC metastasis and cisplatin resistance in vivo

To characterize the function of TEAD4 in vivo, we established a xenograft inguinal lymph node metastasis model and found that the volumes of metastatic inguinal lymph nodes were markedly smaller in xenografts derived from SUNE-1 cells with TEAD4 knockdown than in those of scrambled controls (Fig. 6, A and B). The primary tumors in the TEAD4-knockdown group exhibited sharp edges that expanded as spheroids, indicating a less aggressive phenotype with

the invasion of the skin, muscle, and lymphatic vessels compared with the control group (Fig. 6C). Moreover, the inguinal lymph node metastasis ratio was significantly lower in the TEAD4-knockdown group (Fig. 6, D and E). We further built a lung metastatic colonization model and observed a remarkable reduction in lung metastatic nodules in the TEAD4-knockdown group compared to that in the control group (fig. S19, A and B). Notably, the protein expression of BZW2 was concordantly decreased after the knockdown of TEAD4 in vivo (fig. S19, C and D). In addition, assays in mice showed that subcutaneous xenografts derived from NPC cells with TEAD4 knockdown were much more sensitive to cisplatin treatment than the controls (Fig. 6, F to H). Together, these findings

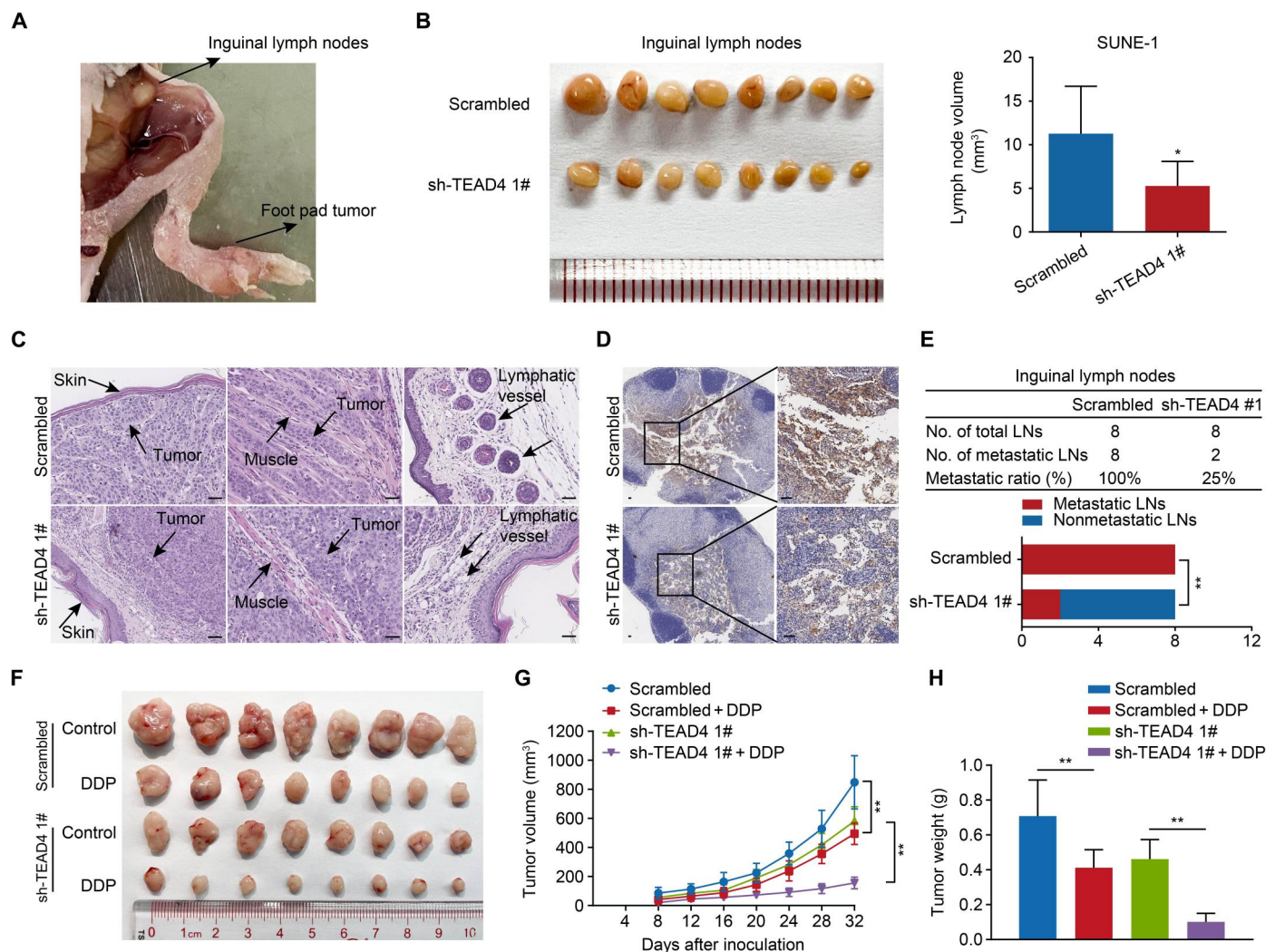


Fig. 6. TEAD4 knockdown decreases NPC cell metastasis and cisplatin resistance in vivo. (A to E) SUNE-1 cells, with or without TEAD4 knockdown, were injected into the footpads of nude mice ($n = 8$ per group) to construct an inguinal lymph node metastasis model. (A) Representative image of the xenograft inguinal lymph node metastasis model. (B) Representative image of the inguinal lymph nodes (left) and the lymph node volume (right). (C) Representative images ($\times 200$) of microscopic primary footpad tumors stained with hematoxylin and eosin. Scale bar, 100 μm . (D) Representative images of immunohistochemistry (IHC) staining of the inguinal lymph nodes with pan-cytokeratin ($\times 40$ and $\times 200$). Scale bar, 100 μm . (E) Inguinal lymph node metastatic ratios. (F to H) SUNE-1 cells, with or without TEAD4 knockdown, were transplanted into the dorsal flank of nude mice to construct a xenograft tumor model. Once the tumor nodes became palpable ($\sim 100 \text{ mm}^3$), mice were randomly divided into four groups ($n = 8$ per group) and injected intraperitoneally with normal saline or cisplatin (DDP; 4 mg/kg) every 4 days. Representative images of xenograft tumors (F), tumor volume growth curves (G), and tumor weight (H) of the xenografts. Tumor volume was compared at indicated time points, and tumor weight was measured at the end point. Data in (B), (G), and (H) are presented as means \pm SD. P values were calculated using unpaired Student's t test (B), Fisher's exact test (E), or one-way ANOVA (G and H). * $P < 0.05$ and ** $P < 0.01$.

indicate that TEAD4 promotes NPC cell metastasis and cisplatin resistance in vivo.

TEAD4 serves as a predictor for prognosis and benefits of cisplatin-based IC in patients in NPC

To gain further insight into the clinical relevance of TEAD4 in NPC, we performed an immunohistochemistry (IHC) analysis in a cohort of NPC samples from Sun Yat-sen University Cancer Center (SYSUCC; cohort 4, $n = 219$) and divided the patients into high and low TEAD4 expression groups (Fig. 7, A and B). By incorporating clinical data, we found that higher TEAD4 expression significantly correlated with a higher risk of disease progression, distant metastasis, and death (table S4). Kaplan-Meier survival analysis and multivariate analysis with a Cox proportional hazards (CPH) model revealed TEAD4 as an independent prognostic indicator for unfavorable disease-free survival, distant metastasis-free survival, and overall survival in patients (Fig. 7, C to E, and table S5). We also evaluated the predictive value of TEAD4 expression for cisplatin-based IC efficacy. In the low TEAD4 expression group, patients who received cisplatin-based IC exhibited significantly better disease control than those who did not, whereas this demonstration of IC benefit was not seen in patients with high TEAD4 expression (Fig. 7, F and G). Furthermore, a treatment-by-covariate interaction test was applied, and a significant interaction between treatment (cisplatin-based IC versus no IC) and TEAD4 levels (high versus low) on survival was identified ($P_{\text{interaction}} = 0.020$; Fig. 7H), supporting the finding that the effects of cisplatin-based IC varied among patients from different TEAD4 expression groups. Together, these findings demonstrate the capability of TEAD4 expression for predicting the prognosis and benefits of cisplatin-based IC in patients with NPC.

DISCUSSION

In this study, we depicted the MR repertoires of high-risk NPC using regulatory network analyses and identified TEAD4 as an MR protein that transcriptionally drives disease progression. Experimental analysis showed that TEAD4 promoted NPC cell migration, invasion, and cisplatin resistance, depending on its autophosphorylation. Furthermore, we demonstrated that YTHDF2 recognizes and stabilizes *TEAD4* transcripts via WTAP-mediated m⁶A modification to facilitate aberrant up-regulation in NPC. The up-regulated TEAD4 further drove malignant phenotypes by promoting BZW2 transcription to induce the oncogenic AKT pathway. Moreover, the transcriptional activity of TEAD4 was independent of YAP/TAZ modulation. We also validated TEAD4 as an independent predictor of unfavorable survival and cisplatin-based IC response in patients with NPC. These results deepen our understanding of the molecular mechanisms of TEAD4 underlying NPC progression and suggest that TEAD4 represents a critical tumor vulnerability for therapeutic intervention.

MR proteins play a crucial role in determining the transcriptional state of cancer cells. They drive multiple malignant phenotypes and therefore have attracted increasing attention in recent years (7–11). Currently, MR proteins have been identified in various cancers (10–12). Nevertheless, in NPC, current knowledge regarding MR proteins remains largely unknown. In the present study, we adopted the VIPER and ARACNe-AP algorithms and identified several MR candidates for high-risk NPC, among which TEAD4

has not yet been investigated in NPC. We then performed experiments to validate the function and clinical relevance of TEAD4 and further uncovered its underlying mechanism in facilitating NPC progression. Specifically, TEAD4 drove NPC migration, invasion, and cisplatin resistance, depending on its autophosphorylation. Mechanistically, it promoted BZW2 transcription to induce the oncogenic AKT pathway. As a canonical transcriptional output of the Hippo-YAP/TAZ pathway, the function of TEAD4 has been widely reported to be dependent on its canonical cofactor YAP/TAZ (18, 19). In NPC, we found that this activity was independent of YAP/TAZ modulation. In line with our observations, YAP/TAZ-independent activity of TEAD4 has also been reported in neuroblastoma and colorectal cancer (10, 37). In addition, a transcriptional activation domain was recently identified in TEAD4, which further supported its function, independent of YAP/TAZ modulation (38).

Furthermore, we found that the aberrant up-regulation of TEAD4 in NPC was driven by m⁶A modification in NPC, in which YTHDF2 recognized WTAP-mediated *TEAD4* m⁶A methylation to facilitate its stability. The m⁶A machinery plays an important role in various carcinogenic processes (24, 39, 40), and recent studies have shown that certain m⁶A regulators (i.e., METTL3, WTAP, and YTHDC2) can promote NPC tumorigenesis or radiotherapy resistance (29, 41, 42). YTHDF2, the first reported m⁶A reader, is widely known for its ability to destabilize m⁶A-modified transcripts (26–28, 40). However, in this study, we identified its ability to destabilize m⁶A-modified *TEAD4* transcripts. This finding is consistent with a recent study by Dixit *et al.* (43) in which YTHDF2 preserved the stability of *MYC* and *VEGFA* transcripts in an m⁶A-dependent manner. Together, these data emphasize the functional complexity of YTHDF2 and expand our knowledge of the role of m⁶A modification in transcript processing during tumorigenesis.

As a critical signaling pathway frequently altered in human cancers, the PI3K-AKT signaling pathway controls the hallmarks of cancer (30). The present study linked TEAD4 activity to AKT pathway activation in NPC, in which TEAD4 exerted its oncogenic effect by promoting BZW2 transcription to induce the AKT pathway. The functional role of BZW2 in regulating the AKT pathway is not yet fully understood, and recent studies have reported that BZW2 promotes tumor proliferation by activating c-Myc or AKT pathways (44–46). Here, we revealed that BZW2 directly regulates PHLPP2, a protein phosphatase involved in AKT inactivation, to induce the AKT pathway and promote NPC progression.

In conclusion, this study uncovered TEAD4 as an MR protein in high-risk NPC and illustrated its important role in NPC progression (Fig. 7I). YTHDF2 recognizes WTAP-mediated *TEAD4* m⁶A methylation to facilitate its stability and leads to aberrant up-regulation of TEAD4 in NPC. Up-regulated TEAD4 expression further promotes NPC metastasis and chemoresistance by transcriptionally promoting the downstream BZW2, which inhibits PHLPP2 to activate the AKT pathway, independent of YAP/TAZ modulation. These findings provide insights into the molecular basis of NPC progression and suggest avenues for the development of predictive biomarkers and therapeutic strategies to improve overall patient survival.

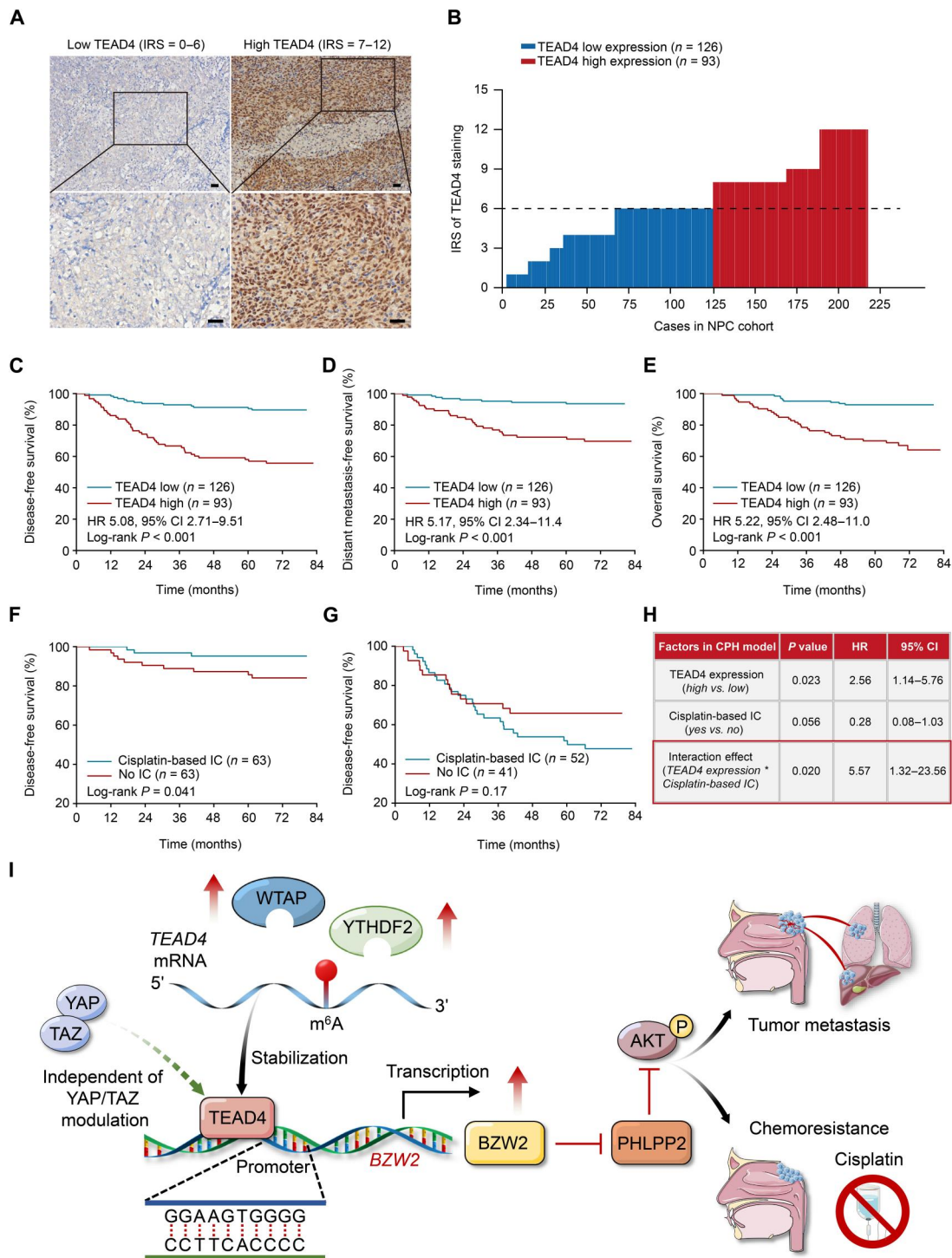


Fig. 7. High expression of TEAD4 is associated with unfavorable prognosis and resistance to cisplatin-based IC in patients with NPC. (A) Representative images of IHC staining for TEAD4 in NPC tissue samples, in which the expression level was measured using the immunoreactive score (IRS) system. Scale bars, 100 μ m. (B) Distribution of TEAD4 IRS in our NPC cohort ($n = 219$). (C to E) Kaplan-Meier curves of disease-free survival (C), distant metastasis-free survival (D), and overall survival (E) according to high and low TEAD4 expression in 219 patients with NPC. Hazard ratios (HRs) were calculated using multivariate analysis with a CPH model (table S5). *P* values were calculated using a log-rank test. (F and G) Kaplan-Meier curves of disease-free survival in patients with NPC from low (F) and high (G) TEAD4 expression groups that were treated with or without cisplatin-based IC. *P* values were calculated using a log-rank test. (H) A treatment-by-covariate (TEAD4 expression * cisplatin-based IC) interaction test with the CPH model on disease-free survival showing that the treatment effect of cisplatin-based IC varied in high versus low TEAD4 expression groups. (I) Proposed working model of TEAD4 in NPC. YTHDF2 recognizes WTAP-mediated TEAD4 m⁶A methylation to facilitate its stability and leads to aberrant up-regulation of TEAD4 in NPC. Up-regulated TEAD4 expression further promotes NPC metastasis and chemoresistance by transcriptionally promoting the downstream BZW2, which inhibits PHLPP2 to activate the AKT pathway, independent of YAP/TAZ modulation.

MATERIALS AND METHODS**Study participants and public datasets**

This study included 219 paraffin-embedded, histopathologically confirmed NPC tissue samples obtained from SYSUCC (Guangzhou, China) between 2011 and 2013 (cohort 4). All patients were treatment-naïve and nonmetastatic at the time of biopsy; their clinical characteristics are presented in table S4. Treatment outcomes included disease-free survival (calculated from the date of treatment to disease failure or death from any cause, whichever occurred first), distant metastasis-free survival (calculated from the date of treatment to distant metastasis), and overall survival (calculated from the date of treatment to death from any cause). Ethical approval was obtained from the Institutional Review Board of the SYSUCC (GZR2018-006) in accordance with the Declaration of Helsinki. The requirement for informed consent was waived owing to the retrospective analysis of anonymous data.

Three publicly available datasets were analyzed in this study. Cohort 1 was previously described by Zhang *et al.* (47) (GSE102349), and 82 patients with nonmetastatic NPC aged between 18 and 70 years with available prognostic information were analyzed. The samples were profiled using bulk RNA-seq, in which the gene expression data were represented as fragments per kilobase of exon model per million mapped fragments, \log_2 -transformed, and filtered to include only genes expressed in at least 50% of the samples. Cohort 2 included 31 NPC tumor tissues and 10 normal nasopharyngeal epithelial tissues profiled by the Affymetrix Human Genome U133 Plus 2.0 Array (GSE12452) (48). Cohort 3 was described in our recent scRNA-seq report (GSE150430) (14), which consisted of 5397 malignant cells profiled by scRNA-seq from six samples with nonmetastatic and histologically proven non-keratinizing NPC (≥ 100 cells per sample). For each malignant cell, we calculated the score of a cell cycling signature using a single-sample GSEA. This cell cycling signature was derived from our scRNA-seq study and reflects cellular aggressiveness (14).

Assembly of transcriptional interactomes and identification of MRs

ARACNe-AP (<http://wiki.c2b2.columbia.edu/califanolab/index.php/Software>) was used to construct transcriptional regulatory network models (i.e., TF-target interactions) from gene expression profiles (13). The TF-target interactions were inferred based on the significance of mutual information between TF genes and candidate target genes, and only edges in the network with $P < 0.05$ after Bonferroni correction were included in the final analysis.

On the basis of the interactome regulons as defined by ARACNe-AP, VIPER analysis was then used to infer protein activity, which was quantified as a normalized enrichment score, which allowed the identification of MRs in certain disease states (i.e., tumor versus normal and progression versus nonprogression) (10, 11). This analysis was performed using the Bioconductor package "vip" (version 1.28.0) (<https://bioconductor.org/packages/release/bioc/html/viper.html>).

Gene set enrichment analysis

GSEA (<http://software.broadinstitute.org/gsea>) was used to identify pathways enriched in the high- versus low-expression groups of *TEAD4* or *BZW2*. The GSEA results are presented as normalized

enrichment scores, and a threshold of $P < 0.05$ and a false discovery rate ≤ 0.25 were used to identify significant pathways.

Cell culture

Immortalized normal human nasopharyngeal epithelial cell lines (NP69 and N2-Tert) were maintained in keratinocyte serum-free medium (Invitrogen), supplemented with bovine pituitary extract (BD Biosciences). Human NPC cell lines (HNE1, HONE-1, SUNE-1, 5-8F, 6-10B, CNE1, and CNE2) were cultured in RPMI 1640 medium (Gibco) supplemented with 10% fetal bovine serum (FBS; Gibco). A549, HeLa, SW620, MDA-MB-231, T24, and HepG2 cells were cultured in Dulbecco's modified Eagle's medium (DMEM; Gibco) supplemented with 10% FBS. The cell lines were authenticated, and normal nasopharyngeal epithelial and NPC cell lines were provided by M.S. Zeng (SYSUCC, China), while HepG2 cells and other cancer cell lines were provided by M.S. Chen (SYSUCC, China) and T.B. Kang (SYSUCC, China), respectively. The human embryonic kidney (HEK) 293T cell line was obtained from the American Type Culture Collection and grown in DMEM (Gibco) supplemented with 10% FBS.

RNA extraction and qRT-PCR

Total RNA was extracted from the cell lines using TRIzol reagent (Invitrogen), and NanoDrop 2000 was used to measure RNA quality and quantity. Reverse transcription was performed using the GoScript Reverse Transcription System (Promega). Next, qRT-PCR was performed using SYBR Green qPCR reagent (Invitrogen) on a CFX96 Touch sequence detection system (Bio-Rad). The normalization control was 18S rRNA for the actinomycin D chase experiment, and glyceraldehyde-3-phosphate dehydrogenase was used as the normalization control for other experiments. The relative expression levels of all the genes were calculated using the $2^{-\Delta\Delta CT}$ method. The specific mRNAs primers used are presented in table S6.

Western blot assays

Cells were lysed on ice in radioimmunoprecipitation assay (RIPA) buffer (Merck Millipore) containing protease and phosphatase inhibitors (Roche, Basel, Switzerland). The protein concentration was assessed using a bicinchoninic acid protein assay kit (Thermo Fisher Scientific). Equal amounts of protein lysates were separated by SDS-polyacrylamide gel electrophoresis (4 to 12%) and then transferred to polyvinylidene fluoride membranes (Merck Millipore). Membranes were blocked with 5% skimmed milk and incubated overnight at 4°C with primary antibodies. The membranes were then incubated with species-matched secondary antibodies at room temperature for 1 hour, and the proteins were detected using BeyoECL Plus (Beyotime). Information on the primary antibodies used is shown in table S7.

Transient transfection and generation of stably transfected cell lines

For RNA interference, duplex RNA interference oligonucleotides targeting human *YTHDF1* to *YTHDF3*, *WTAP*, *IGF2BP1* to *IGF2BP3*, *PHLPP2*, *YAP*, and *TAZ* mRNA sequences were synthesized and purchased from GenePharma (Suzhou, China). A scrambled duplex RNA oligonucleotide was used as a negative control. Sequences are listed in table S8. An online tool (GPP web Portal) was used to design short hairpin RNAs (shRNAs) against *TEAD4*

and BZW2. The synthesized sequences listed in table S9 were cloned into a pLKO vector. TEAD1, TEAD2, TEAD3, HA- or Myc-tagged TEAD4, Myc-tagged mutant TEAD4, and BZW2 constructs were cloned into a pSin-EF2-puro plasmid. Site-directed mutagenesis was performed using bridge PCR, and sequencing was performed for confirmation. Cells were transfected with Lipofectamine 3000 (Invitrogen), according to the manufacturer's protocol, and harvested for assays after transfection for 48 hours. SUNE-1 and HONE-1 cell lines with stable knockdown or overexpression were generated via lentiviral infection in HEK293T cells. Stable clones were selected using puromycin and confirmed through qRT-PCR and Western blot assays.

Wound healing assay

For wound healing assays, transfected SUNE-1 and HONE-1 cells were seeded in six-well plates and cultured in the suffusion state. Then, all cells were cultured in a serum-free medium for 24 hours. Linear wounds were created in cell monolayers by scraping with a P-200 pipette tip. Cells that detached from the bottom of the wells were washed with phosphate-buffered saline (PBS), and the remaining cells were cultured in a serum-free medium for another 24 hours (starvation). Images were captured with an inverted microscope (Olympus IX73), and the width of the scratch was quantified to compare the migratory ability among the different groups.

Transwell migration and invasion assays

For Transwell migration and invasion assays, transwell chambers (8 μm pores; Corning) were coated with or without Matrigel (BD Biosciences). Subsequently, SUNE-1 (5×10^4) or HONE-1 (3.5×10^4) cells suspended in serum-free medium (200 μl) were seeded into the upper chambers without Matrigel, and SUNE-1 (1×10^5) or HONE-1 (7×10^4) cells suspended in 200 μl of serum-free medium were seeded into the upper chambers with Matrigel. All lower chambers were filled with 500 μl of medium supplemented with 10% FBS. After incubation for 16 hours (Transwell migration) or 22 hours (Transwell invasion), the migrated or invaded cells were fixed with methanol, stained with hematoxylin, and counted under an inverted microscope.

Cell viability and colony formation assays

For the cell viability assay, 1×10^3 cells per well were seeded in a 96-well plate in full medium supplemented with 10% FBS and cultured for 0 to 4 days. Cell viability was measured every 24 hours using a CCK-8 kit (Dojindo). Absorbance was measured at 450 nm using a spectrophotometric plate reader (BioTek ELX800, Bio-Rad). For colony formation assay, cells were seeded in six-well plates (400 cells per well) and cultured for approximately 7 days for HONE-1 cells and 14 days for SUNE-1 cells, until colonies were detectable. The cells were then fixed, stained, and analyzed.

Cisplatin treatment and cell apoptosis assay

For cisplatin treatment, SUNE-1 and HONE-1 cells (1000 cells in 200 μl medium per well) were seeded in 96-well plates and incubated with cisplatin (0, 0.625, 1.25, 2.5, 5, and 10 $\mu\text{g}/\text{ml}$) for 72 hours. Then, 20 μl of CCK-8 reagent was added to each well and incubated at 37°C for another 2 hours. The absorbance per well was read on the spectrophotometer at 450 nm. For cell apoptosis assay, cells treated with cisplatin (20 μM) for 30 hours were dissociated using

0.25% trypsin (EDTA-free). Each sample was resuspended in 300 μl of binding buffer and incubated with 2.5 μl of annexin V and 3 μl of 7AAD (7-Aminoactinomycin D) fluorescent dye. The apoptosis rate was detected using a CytExpert flow cytometer and analyzed using the FlowJo software. APC⁺/7AAD⁺ cells were considered late apoptotic or dead cells, APC⁺/7AAD⁻ cells were considered early apoptotic cells, and APC⁻/7AAD⁻ cells were considered viable cells.

Acyl-biotin exchange assay

Palmitoylation of proteins was analyzed using acyl-biotin exchange (ABE) assays as previously described, with some modifications (49, 50). SUNE-1 cells treated with MGH-CP1 (S9735, Selleck) or transiently expressing Myc-tagged wild-type or palmitoylation-deficient (C335S, C367A) TEAD4 were subjected to ABE assay. Briefly, cells were collected, and proteins were extracted and incubated in 50 mM *N*-ethylmaleimide (Sigma-Aldrich) diluted in RIPA buffer at 4°C with rotation for 1 hour and then incubated with anti-TEAD4 (ab58310, Abcam) or anti-Myc antibody (2276S, Cell Signaling Technology) at 4°C overnight. Protein A/G magnetic beads (88802, Thermo Fisher Scientific) were added to each reaction and incubated at room temperature for 1 hour. The beads were then washed five times with lysis buffer. Each sample was divided into two equal parts: one part included the hydroxylamine (HAM) step, which was incubated with HAM (1 M; 467804, Millipore Sigma) containing lysis buffer at room temperature with rotating for 1 hour (+HAM sample), and the other part was treated identically without HAM (-HAM sample). After washing five times, the beads were treated with a thiol-reactive biotin molecule, Biotin-BMCC (C100222-0050, Sangon Biotech). Then, all samples were washed. Last, the immunoprecipitated samples were analyzed by immunoblotting using anti-TEAD4 or anti-Myc antibodies.

m⁶A site prediction and MeRIP-qPCR

The online prediction tool SRAMP (www.cuilab.cn/sramp) was used to predict the potential m⁶A sites (25). The MeRIP assay was performed using a procedure provided by the Millipore Magna MeRIP m⁶A Kit (17-10499, Millipore). Briefly, total RNA (300 μg) was extracted from NP69, SUNE-1, and HONE-1 cells and incubated at 94°C for 2 min for fragmentation. One-tenth of the RNA was saved as the "RNA input." Anti-m⁶A antibody (10 μg) or anti-immunoglobulin G (IgG; 10 μg) was incubated with washed A/G blend magnetic beads (50 μl) at room temperature for 30 min. The fragmented RNA was then incubated with m⁶A antibody-associated beads at 4°C for 2 hours with rotation. After three washes, RNA was extracted from the beads using an RNA Purification Kit. Last, equal volumes of purified RNA were used for reverse transcription PCR and quantified using qRT-PCR.

RNA pull-down assay

Full-length *TEAD4* transcripts, the *TEAD4* CDS region, and m⁶A motif-depleted CDS regions were cloned into the pcDNA3.1. RNA was transcribed in vitro using a MEGAscript T7 Transcription Kit (AM1333, Thermo Fisher Scientific). The amplified RNA was then purified and labeled with biotin using a Pierce RNA 3' End Desthiobiotinylation Kit (20163, Thermo Fisher Scientific). Last, RNA pull-down was performed using the Pierce Magnetic RNA-Protein Pull-Down Kit (20164, Thermo Fisher Scientific), following the manufacturer's instructions. Briefly, cell lysates were incubated

with streptavidin magnetic beads conjugated with biotinylated linearized TEAD4 mRNAs or truncated versions (CDS wild-type and CDS m⁶A motif depletion), and the interaction between YTHDF2 and TEAD4 transcripts was determined by Western blotting. Specific sequences are listed in table S10.

RIP assay

RIP assays were performed using the Magna RIP Kit (17-700, Millipore), according to the manufacturer's instructions. First, the cells were lysed in RIP lysis buffer supplemented with protease and ribonuclease inhibitors. The cell lysates were incubated with magnetic beads conjugated with anti-YTHDF2 (5 µg) or anti-IgG (5 µg) antibodies on a rotator at 4°C overnight. After immunoprecipitation, the supernatant was discarded, and the beads with specific RNA-protein complexes were washed six times with RIP wash buffer. The magnetic beads were then incubated with proteinase K, followed by the phenol-chloroform method for RNA purification. Last, the interaction between YTHDF2 and TEAD4 transcripts was determined using qPCR and normalized to the input.

ChIP assays

The ChIP assay was performed according to the Pierce Magnetic ChIP Kit protocol (26157, Thermo Fisher Scientific). Briefly, cells were cross-linked and the nucleoprotein complexes were sheared to yield 200- to 500-bp DNA fragments by sonication. The DNA fragments were immunoprecipitated with anti-HA (ab9110, Abcam), anti-TEAD4 (ab58310, Abcam), or anti-BZW2 (21001-1-AP, Proteintech) antibodies. For ChIP-seq analysis, purified DNA fragments were sequenced at the Beijing Genomics Institute. Sequences of the qRT-PCR primers used for ChIP-qPCR analysis are listed in table S11.

Dual-luciferase reporter assay

Wild-type and mutant promoters of BZW2 or PHLPP2 (2000 bp upstream of the transcription start site) were cloned into pGL3-basic luciferase reporter plasmids (Promega). SUNE-1 and HONE-1 cells were seeded into 24-well plates and cotransfected with plasmids encoding an empty vector or TEAD4 along with BZW2 wild-type or mutant promoter-reporter plasmids (100 ng), or plasmids encoding an empty vector or BZW2 along with PHLPP2 promoter-reporter plasmids (100 ng), and a Renilla luciferase reporter (10 ng) using Lipofectamine 3000 (L3000015, Invitrogen). Cells were lysed after incubation for 36 hours. Luciferase activity was detected using the Dual-Luciferase Reporter Assay System (E1910, Promega), and firefly luciferase activity was normalized to Renilla luciferase activity.

Co-IP assay

Cells were lysed in IP lysis buffer (Thermo Fisher Scientific) containing protease and phosphatase inhibitors (Roche, Basel, Switzerland) and sonicated. Cell lysates were incubated with anti-YAP (13584-1-AP, Proteintech), anti-TAZ (23306-1-AP, Proteintech), or anti-Myc (2276S, Cell Signaling Technology) antibodies at 4°C overnight. The immunocomplexes were added to washed Protein A/G magnetic beads (88802, Thermo Fisher Scientific) and incubated at room temperature for 1 hour. Last, the beads were washed five times with IP lysis buffer and subjected to Western blot analysis.

Gel filtration chromatography analysis

Gel filtration chromatography was performed on a Superdex 75 10/300 column (GE Healthcare) using an AKTA purifier system (GE Healthcare) with UNICORN 5.31 (build 743) workstation software. The protein extract was loaded onto the column and separated in gel filtration buffer [50 mM Hepes (pH 7.5), 150 mM NaCl, and 1 mM dithiothreitol] at 4°C. The flow rate was 0.4 ml/min, and the fractions were 0.5 ml per tube. In total, 48 fractions (A1 to A12, B1 to B12, C1 to C12, and D1 to D12) were collected for Western blot analysis.

CRISPR genome editing

To generate YAP/TAZ double-knockout cells, optimal single-guide RNA (sgRNA) target sequences were designed using Benchling. The sgRNA target sequences for YAP or TAZ (table S12) were separately cloned into a PX458 plasmid. First, cells were transfected with a plasmid targeting YAP and sorted, and knockout efficiency was validated by Western blot assays. TAZ was then knocked out in YAP-knockout cells using the same method described above.

In vivo nude mouse models

All animal experiments were performed in accordance with the guidelines of the Institutional Animal Care and Use Ethics Committee of SYSUCC (L102012018000G). BALB/c nude mice (female, 4 to 6 weeks old) were obtained from Charles River Laboratories (Beijing, China) and maintained at the Animal Experiment Center of the Sun Yat-sen University.

For the inguinal lymph node metastasis model (51), 30 µl of PBS containing SUNE-1 cells (2×10^5) stably expressing shTEAD4 or control shRNA was inoculated into mouse footpads ($n = 8$ per group). Six weeks later, the mice were euthanized and their inguinal lymph nodes were detached for further analysis.

For the lung metastasis model, 200 µl of PBS containing SUNE-1 cells (1×10^6) stably expressing shTEAD4 or control shRNA was injected into mice via the tail vein ($n = 6$ per group). After 8 weeks of growth, the mice were euthanized and their lung tissues were dissected. All dissected tissue samples were embedded in paraffin, sectioned, and stained with hematoxylin and eosin. In addition, IHC staining was performed on inguinal lymph nodes using an anti-pan-cytokeratin antibody (Thermo Fisher Scientific) and lung tissues using antibodies against TEAD4 (ab58310, 1:100; Abcam) and BZW2 (HPA022813, 1:500; Atlas Antibody).

For the subcutaneous xenograft tumor growth model, 1×10^6 SUNE-1 cells (stably silenced for TEAD4 or control cells) suspended in 200 µl of PBS were injected into the mice's dorsal flank. Once the tumor nodes became palpable ($\sim 100 \text{ mm}^3$), the mice in each group (sh-scrambled and sh-TEAD4) were randomly subdivided into two subsets ($n = 8$ in each subset) and intraperitoneally injected with cisplatin (4 mg/kg) or normal saline every 4 days. Tumor diameters were measured every 4 days. The mice were euthanized on day 32, and the tumors were dissected and weighed.

Immunohistochemistry

Briefly, the tissue sections were deparaffinized; rehydrated; subjected to endogenous peroxidase activity blocking, high-temperature antigen retrieval, and nonspecific binding blocking; and incubated with primary antibodies. The following day, the sections were incubated with the appropriate secondary antibodies for 30 min at 37°C, visualized by staining with 3,3'-diaminobenzidine (DAB),

counterstained with hematoxylin, dehydrated, and covered with a coverslip. Images were captured using a NIKON ECLIPSE 80i microscope (Japan). For TEAD4 and BZW2, two pathologists evaluated the staining intensity and proportion of positive cells using the immunoreactive score (IRS) system. The staining intensity was defined as follows: 0, no staining; 1, weak, light yellow; 2, moderate, yellow-brown; and 3, strong, brown. The proportion of positive cells was defined as follows: 1, <10%; 2, 10 to 35%; 3, 36 to 70%; and 4, >70%. IRS scores were calculated as the product of the staining intensity scores and the proportion of positive cells.

Statistical analysis

Unless otherwise stated, the unpaired Student's *t* test or Wilcoxon rank sum test was used to compare continuous variables between two groups, one-way analysis of variance (ANOVA) was used to compare continuous variables between several groups, and the χ^2 test or Fisher's exact test was used to compare categorical variables. The strength of the relationship was evaluated using Pearson's correlation analysis. The Kaplan-Meier method was used to plot survival curves, and differences were compared using the log-rank test. Multivariate analysis with a CPH model was used to calculate hazard ratios and determine independent prognostic factors. Further treatment-by-covariate interaction analysis with the CPH model was used to assess whether the treatment effect of IC varied in the high versus low TEAD4 expression groups. Statistical analyses were conducted using R version 4.0.2 (www.r-project.org), SPSS (version 22.0; IBM, Armonk, NY, USA), or GraphPad Prism version 8.0 (GraphPad Inc., La Jolla, CA, USA). Error bars indicate SD as mentioned in figure legends for a minimum of three independent experiments. All *P* < 0.05 were considered statistically significant.

Supplementary Materials

This PDF file includes:

Figs. S1 to S19
Tables S4 to S12

Other Supplementary Material for this manuscript includes the following:

Tables S1 to S3

[View/request a protocol for this paper from Bio-protocol.](#)

REFERENCES AND NOTES

1. Y. P. Chen, A. T. C. Chan, Q.-T. Le, P. Blanchard, Y. Sun, J. Ma, Nasopharyngeal carcinoma. *Lancet* **394**, 64–80 (2019).
2. Y. P. Chen, N. Ismaila, M. L. K. Chua, A. D. Colevas, R. Haddad, S. H. Huang, J. T. S. Wee, A. C. Whitley, J. L. Yi, S. S. Yom, A. T. C. Chan, C. S. Hu, J. Y. Lang, Q. T. Le, A. W. M. Lee, N. Lee, J. C. Lin, B. Ma, T. J. Morgan, J. Shah, Y. Sun, J. Ma, Chemotherapy in combination with radiotherapy for definitive-intent treatment of stage II-IVA nasopharyngeal carcinoma: CSCO and ASCO Guideline. *J. Clin. Oncol.* **39**, 840–859 (2021).
3. L. L. Tang, Y. P. Chen, C. B. Chen, M. Y. Chen, N. Y. Chen, X. Z. Chen, X. J. Du, W. F. Fang, M. Feng, J. Gao, F. Han, X. He, C. S. Hu, D. S. Hu, G. Y. Hu, H. Jiang, W. Jiang, F. Jin, J. Y. Lang, J. G. Li, S. J. Lin, X. Liu, Q. F. Liu, L. Ma, H. Q. Mai, J. Y. Qin, L. F. Shen, Y. Sun, P. G. Wang, R. S. Wang, R. Z. Wang, X. S. Wang, Y. Wang, H. Wu, Y. F. Xia, S. W. Xiao, K. Y. Yang, J. L. Yi, X. D. Zhu, J. Ma, The Chinese Society of Clinical Oncology (CSCO) clinical guidelines for the diagnosis and treatment of nasopharyngeal carcinoma. *Cancer Commun.* **41**, 1195–1227 (2021).
4. J. P. Bruce, K. Yip, S. V. Bratman, E. Ito, F. F. Liu, Nasopharyngeal cancer: Molecular landscape. *J. Clin. Oncol.* **33**, 3346–3355 (2015).
5. K. C. W. Wong, E. P. Hui, K. W. Lo, W. K. J. Lam, D. Johnson, L. Li, Q. Tao, K. C. A. Chan, K. F. To, A. D. King, B. B. Y. Ma, A. T. C. Chan, Nasopharyngeal carcinoma: An evolving paradigm. *Nat. Rev. Clin. Oncol.* **18**, 679–695 (2021).
6. Y. Zhang, L. Chen, G. Q. Hu, N. Zhang, X. D. Zhu, K. Y. Yang, F. Jin, M. Shi, Y. P. Chen, W. H. Hu, Z. B. Cheng, S. Y. Wang, Y. Tian, X. C. Wang, Y. Sun, J. G. Li, W. F. Li, Y. H. Li, L. L. Tang, Y. P. Mao, G. Q. Zhou, R. Sun, X. Liu, R. Guo, G. X. Long, S. Q. Liang, L. Li, J. Huang, J. H. Long, J. Zhang, Q. D. Liu, L. Zou, Q. F. Su, B. M. Zheng, Y. Xiao, Y. Guo, F. Han, H. Y. Mo, J. W. Lv, X. J. Du, C. Xu, N. Liu, Y. Q. Li, M. L. K. Chua, F. Y. Xie, Y. Sun, J. Ma, Gemcitabine and cisplatin induction chemotherapy in nasopharyngeal carcinoma. *N. Engl. J. Med.* **381**, 1124–1135 (2019).
7. A. Califano, M. J. Alvarez, The recurrent architecture of tumour initiation, progression and drug sensitivity. *Nat. Rev. Cancer* **17**, 116–130 (2017).
8. M. J. Alvarez, P. S. Subramaniam, L. H. Tang, A. Grunn, M. Aburi, G. Rieckhof, E. V. Komisarova, E. A. Hagan, L. Bodei, P. A. Clemons, F. S. Dela Cruz, D. Dhall, D. Diolaiti, D. A. Fraker, A. Ghavami, D. Kaemmerer, C. Karan, M. Kidd, K. M. Kim, H. C. Kim, L. P. Kunju, U. Langel, Z. Li, J. Lee, H. Li, V. LiVolsi, R. Pfragner, A. R. Rainey, R. B. Realubit, H. Remotti, J. Regberg, R. Roses, A. Rustgi, A. R. Sepulveda, S. Serra, C. Shi, X. Yuan, M. Barberis, R. Bergamaschi, A. M. Chinnaiyan, T. Detre, S. Ezzat, A. Frilling, M. Hommann, D. Jaeger, M. K. Kim, B. S. Knudsen, A. L. Kung, E. Leahy, D. C. Metz, J. W. Milsom, Y. S. Park, D. Reidy-Lagunes, S. Schreiber, K. Washington, B. Wiedenmann, I. Modlin, A. Califano, A precision oncology approach to the pharmacological targeting of mechanistic dependencies in neuroendocrine tumors. *Nat. Genet.* **50**, 979–989 (2018).
9. B. Bisikirska, M. Bansal, Y. Shen, J. Teruya-Feldstein, R. Chaganti, A. Califano, Elucidation and pharmacological targeting of novel molecular drivers of follicular lymphoma progression. *Cancer Res.* **76**, 664–674 (2016).
10. P. Rajbhandari, G. Lopez, C. Capdevila, B. Salvatori, J. Yu, R. Rodriguez-Barrueco, D. Martinez, M. Yarmarkovich, N. Weichert-Leahey, B. J. Abraham, M. J. Alvarez, A. Iyer, J. L. Harenza, D. Oldridge, K. De Preter, J. Koster, S. Asgharzadeh, R. C. Seeger, J. S. Wei, J. Khan, J. Vandesompele, P. Mestdagh, R. Versteeg, A. T. Look, R. A. Young, A. Iavarone, A. Lasorella, J. M. Silva, J. M. Maris, A. Califano, Cross-cohort analysis identifies a TEAD4-MYCN positive feedback loop as the core regulatory element of high-risk neuroblastoma. *Cancer Discov.* **8**, 582–599 (2018).
11. M. J. Alvarez, Y. Shen, F. M. Giorgi, A. Lachmann, B. B. Ding, B. H. Ye, A. Califano, Functional characterization of somatic mutations in cancer using network-based inference of protein activity. *Nat. Genet.* **48**, 838–847 (2016).
12. E. O. Paull, A. Aytes, S. J. Jones, P. S. Subramaniam, F. M. Giorgi, E. F. Douglass, S. Tagore, B. Chu, A. Vasciaveo, S. Zheng, R. Verhaak, C. Abate-Shen, M. J. Alvarez, A. Califano, A modular master regulator landscape controls cancer transcriptional identity. *Cell* **184**, 334–351.e20 (2021).
13. A. Lachmann, F. M. Giorgi, G. Lopez, A. Califano, ARACNe-AP: Gene network reverse engineering through adaptive partitioning inference of mutual information. *Bioinformatics* **32**, 2233–2235 (2016).
14. Y. Chen, J. Yin, W. Li, H. Li, D. Chen, C. Zhang, J. Lv, Y. Wang, X. Li, J. Li, P. Zhang, Y. Li, Q. He, X. Yang, Y. Lei, L. Tang, G. Zhou, Y. Mao, C. Wei, K. Xiong, H. Zhang, S. Zhu, Y. Hou, Y. Sun, M. Dean, I. Amit, K. Wu, D. Kuang, G. Li, N. Liu, J. Ma, Single-cell transcriptomics reveals regulators underlying immune cell diversity and immune subtypes associated with prognosis in nasopharyngeal carcinoma. *Cell Res.* **30**, 1024–1042 (2020).
15. H. Chen, C. Yang, L. Yu, L. Xie, J. Hu, L. Zeng, Y. Tan, Adenovirus-mediated RNA interference targeting FOXM1 transcription factor suppresses cell proliferation and tumor growth of nasopharyngeal carcinoma. *J. Gene Med.* **14**, 231–240 (2012).
16. Y. Li, Q. He, X. Wen, X. Hong, X. Yang, X. Tang, P. Zhang, Y. Lei, Y. Sun, J. Zhang, Y. Wang, J. Ma, N. Liu, EZH2-DNMT1-mediated epigenetic silencing of miR-142-3p promotes metastasis through targeting ZEB2 in nasopharyngeal carcinoma. *Cell Death Differ.* **26**, 1089–1106 (2019).
17. P. Liu, X. Zhang, Z. Li, L. Wei, Q. Peng, C. Liu, Y. Wu, Q. Yan, J. Ma, A significant role of transcription factors E2F in inflammation and tumorigenesis of nasopharyngeal carcinoma. *Biochem. Biophys. Res. Commun.* **524**, 816–824 (2020).
18. A. Dey, X. Varelas, K. L. Guan, Targeting the Hippo pathway in cancer, fibrosis, wound healing and regenerative medicine. *Nat. Rev. Drug Discov.* **19**, 480–494 (2020).
19. K. C. Lin, H. W. Park, K. L. Guan, Regulation of the Hippo pathway transcription factor TEAD. *Trends Biochem. Sci.* **42**, 862–872 (2017).
20. Y. Mesrouze, M. Meyerhofer, F. Bokhovchuk, P. Fontana, C. Zimmermann, T. Martin, C. Delaunay, A. Izaac, J. Kallen, T. Schmelzle, D. Erdmann, P. Chene, Effect of the acylation of TEAD4 on its interaction with co-activators YAP and TAZ. *Protein Sci.* **26**, 2399–2409 (2017).
21. N. G. Kim, B. M. Gumbiner, Cell contact and Nf2/Merlin-dependent regulation of TEAD palmitoylation and activity. *Proc. Natl. Acad. Sci. U.S.A.* **116**, 9877–9882 (2019).
22. Q. Li, Y. Sun, G. K. Jarugumilli, S. Liu, K. Dang, J. L. Cotton, J. Xiol, P. Y. Chan, M. DeRan, L. Ma, R. Li, L. J. Zhu, J. H. Li, A. B. Leiter, Y. T. Ip, F. D. Camargo, X. Luo, R. L. Johnson, X. Wu, J. Mao, Lats1/2 sustain intestinal stem cells and Wnt activation through TEAD-dependent and independent transcription. *Cell Stem Cell* **26**, 675–692.e8 (2020).

23. W. Jiang, N. Liu, X. Z. Chen, Y. Sun, B. Li, X. Y. Ren, W. F. Qin, N. Jiang, Y. F. Xu, Y. Q. Li, J. Ren, W. C. Cho, J. P. Yun, J. Zeng, L. Z. Liu, L. Li, Y. Guo, H. Q. Mai, M. S. Zeng, T. B. Kang, W. H. Jia, J. Y. Shao, J. Ma, Genome-wide identification of a methylation gene panel as a prognostic biomarker in nasopharyngeal carcinoma. *Mol. Cancer Ther.* **14**, 2864–2873 (2015).
24. D. Dominissini, S. Moshitch-Moshkovitz, S. Schwartz, M. Salmon-Divon, L. Ungar, S. Osenberg, K. Cesarkas, J. Jacob-Hirsch, N. Amariglio, M. Kupiec, R. Sorek, G. Rechavi, Topology of the human and mouse m6A RNA methylomes revealed by m6A-seq. *Nature* **485**, 201–206 (2012).
25. Y. Zhou, P. Zeng, Y. H. Li, Z. Zhang, Q. Cui, SRAMP: Prediction of mammalian N6-methyladenosine (m6A) sites based on sequence-derived features. *Nucleic Acids Res.* **44**, e91 (2016).
26. X. Wang, Z. Lu, A. Gomez, G. C. Hon, Y. Yue, D. Han, Y. Fu, M. Parisien, Q. Dai, G. Jia, B. Ren, T. Pan, C. He, N6-methyladenosine-dependent regulation of messenger RNA stability. *Nature* **505**, 117–120 (2014).
27. H. Du, Y. Zhao, J. He, Y. Zhang, H. Xi, M. Liu, J. Ma, L. Wu, YTHDF2 destabilizes m(6)A-containing RNA through direct recruitment of the CCR4-NOT deadenylase complex. *Nat. Commun.* **7**, 12626 (2016).
28. L. J. Deng, W. Q. Deng, S. R. Fan, M. F. Chen, M. Qi, W. Y. Lyu, Q. Qi, A. K. Tiwari, J. X. Chen, D. M. Zhang, Z. S. Chen, m6A modification: Recent advances, anticancer targeted drug discovery and beyond. *Mol. Cancer* **21**, 52 (2022).
29. Z. X. Li, Z. Q. Zheng, P. Y. Yang, L. Lin, G. Q. Zhou, J. W. Lv, L. L. Zhang, F. Chen, Y. Q. Li, C. F. Wu, F. Li, J. Ma, N. Liu, Y. Sun, WTAP-mediated m(6)A modification of lncRNA DIAPH1-AS1 enhances its stability to facilitate nasopharyngeal carcinoma growth and metastasis. *Cell Death Differ.* **29**, 1137–1151 (2022).
30. Y. He, M. M. Sun, G. G. Zhang, J. Yang, K. S. Chen, W. W. Xu, B. Li, Targeting PI3K/Akt signal transduction for cancer therapy. *Signal Transduct. Target. Ther.* **6**, 425 (2021).
31. B. Nachmias, D. H. Khan, V. Voisin, A. S. Mer, G. E. Thomas, N. Segev, J. St-Germain, R. Hurren, M. Gronda, A. Botham, X. Wang, N. Maclean, A. K. Seneviratne, N. Duong, C. Xu, A. Arruda, E. Oruji, A. Alگونهh, R. Hakem, L. Shlush, M. D. Minden, B. Raught, G. D. Bader, A. D. Schimmer, IPO11 regulates the nuclear import of BZW1/2 and is necessary for AML cells and stem cells. *Leukemia* **36**, 1283–1295 (2022).
32. J. Brognard, E. Sierecki, T. Gao, A. C. Newton, PHLPP and a second isoform, PHLPP2, differentially attenuate the amplitude of Akt signaling by regulating distinct Akt isoforms. *Mol. Cell* **25**, 917–931 (2007).
33. D. G. Nowak, H. Cho, T. Herzka, K. Watrud, D. V. DeMarco, V. M. Wang, S. Senturk, C. Fellmann, D. Ding, T. Beinortas, D. Kleinman, M. Chen, R. Sordella, J. E. Wilkinson, M. Castillo-Martin, C. Cordon-Cardo, B. D. Robinson, L. C. Trotman, MYC drives Pten/Trp53-deficient proliferation and metastasis due to IL6 secretion and AKT suppression via PHLPP2. *Cancer Discov.* **5**, 636–651 (2015).
34. J. Shen, Q. Huang, W. Jia, S. Feng, L. Liu, X. Li, D. Tao, D. Xie, YAP1 induces invadopodia formation by transcriptionally activating TIAM1 through enhancer in breast cancer. *Oncogene* **41**, 3830–3845 (2022).
35. Y. Wu, Q. Zheng, Y. Li, G. Wang, S. Gao, X. Zhang, X. Yan, X. Zhang, J. Xie, Y. Wang, X. Sun, X. Meng, B. Yin, B. Wang, Metformin targets a YAP1-TEAD4 complex via AMPK α to regulate CCNE1/2 in bladder cancer cells. *J. Exp. Clin. Cancer Res.* **38**, 376 (2019).
36. L. Chen, S. W. Chan, X. Zhang, M. Walsh, C. J. Lim, W. Hong, H. Song, Structural basis of YAP recognition by TEAD4 in the hippo pathway. *Genes Dev.* **24**, 290–300 (2010).
37. Y. Liu, G. Wang, Y. Yang, Z. Mei, Z. Liang, A. Cui, T. Wu, C. Y. Liu, L. Cui, Increased TEAD4 expression and nuclear localization in colorectal cancer promote epithelial-mesenchymal transition and metastasis in a YAP-independent manner. *Oncogene* **35**, 2789–2800 (2016).
38. C. Qiao, Y. Jiang, C. Deng, Z. Huang, K. Teng, L. Chen, X. Liu, Characterization of the transcriptional activation domains of human TEF3-1 (transcription enhancer factor 3 isoform 1). *Arch. Biochem. Biophys.* **569**, 54–61 (2015).
39. G. W. Kim, H. Imam, M. Khan, S. A. Mir, S. J. Kim, S. K. Yoon, W. Hur, A. Siddiqui, HBV-induced increased N6 methyladenosine modification of PTEN RNA affects innate immunity and contributes to HCC. *Hepatology* **73**, 533–547 (2021).
40. H. Huang, H. Weng, J. Chen, m(6)A modification in coding and non-coding RNAs: Roles and therapeutic implications in cancer. *Cancer Cell* **37**, 270–288 (2020).
41. P. Zhang, Q. He, Y. Lei, Y. Li, X. Wen, M. Hong, J. Zhang, X. Ren, Y. Wang, X. Yang, Q. He, J. Ma, N. Liu, m(6)A-mediated ZNF750 repression facilitates nasopharyngeal carcinoma progression. *Cell Death Dis.* **9**, 1169 (2018).
42. J. J. He, Z. Li, Z. X. Rong, J. Gao, Y. Mu, Y. D. Guan, X. X. Ren, Y. Y. Zi, L. Y. Liu, Q. Fan, M. Zhou, Y. M. Duan, Q. Zhou, Y. Z. Deng, L. Q. Sun, m(6)A reader YTHDC2 promotes radiotherapy resistance of nasopharyngeal carcinoma via activating IGF1R/AKT/S6 signaling axis. *Front. Oncol.* **10**, 1166 (2020).
43. D. Dixit, B. C. Prager, R. C. Gimple, H. X. Poh, Y. Wang, Q. Wu, Z. Qiu, R. L. Kidwell, L. J. Y. Kim, Q. Xie, K. Vitting-Seerup, S. Bhargava, Z. Dong, L. Jiang, Z. Zhu, P. Hamerlik, S. R. Jaffrey, J. C. Zhao, X. Wang, J. N. Rich, The RNA m6A reader YTHDF2 maintains oncogene expression and is a targetable dependency in glioblastoma stem cells. *Cancer Discov.* **11**, 480–499 (2021).
44. D. D. Cheng, S. J. Li, B. Zhu, T. Yuan, Q. C. Yang, C. Y. Fan, Downregulation of BZW2 inhibits osteosarcoma cell growth by inactivating the Akt/mTOR signaling pathway. *Oncol. Rep.* **38**, 2116–2122 (2017).
45. K. Sato, T. Masuda, Q. Hu, T. Toba, S. Gillaspie, A. Niida, M. Thornton, Y. Kuroda, H. Eguchi, T. Nakagawa, K. Asano, K. Mimori, Novel oncogene 5MP1 reprograms c-Myc translation initiation to drive malignant phenotypes in colorectal cancer. *EBioMedicine* **44**, 387–402 (2019).
46. G. Li, A. Lu, A. Chen, S. Geng, Y. Xu, X. Chen, J. Yang, BZW2/5MP1 acts as a promising target in hepatocellular carcinoma. *J. Cancer* **12**, 5125–5135 (2021).
47. L. Zhang, K. D. MacIsaac, T. Zhou, P. Y. Huang, C. Xin, J. R. Dobson, K. Yu, D. Y. Chiang, Y. Fan, M. Pelletier, Y. Wang, S. Jaeger, V. Krishnamurthy Radhakrishnan, L. JeBailey, P. Skewes-Cox, J. Zhang, W. Fang, Y. Huang, H. Zhao, Y. Zhao, E. Li, B. Peng, A. Huang, G. Dranoff, P. S. Hammerman, J. Engelman, H. Bitter, Y. X. Zeng, Y. Yao, Genomic analysis of nasopharyngeal carcinoma reveals TME-based subtypes. *Mol. Cancer Res.* **15**, 1722–1732 (2017).
48. S. Sengupta, J. A. den Boon, I. H. Chen, M. A. Newton, D. B. Dahl, M. Chen, Y.-J. Cheng, W. H. Westra, C.-J. Chen, A. Hildesheim, B. Sugden, P. Ahlquist, Genome-wide expression profiling reveals EBV-associated inhibition of MHC class I expression in nasopharyngeal carcinoma. *Cancer Res.* **66**, 7999–8006 (2006).
49. L. Zhou, X. He, L. Wang, P. Wei, Z. Cai, S. Zhang, S. Jin, H. Zeng, J. Cui, Palmitoylation restricts SQSTM1/p62-mediated autophagic degradation of NOD2 to modulate inflammation. *Cell Death Differ.* **29**, 1541–1551 (2022).
50. X. Ge, Z. He, C. Cao, T. Xue, J. Jing, R. Ma, W. Zhao, L. Liu, K. Jueraitibaik, J. Ma, Y. Feng, Z. Qian, Z. Zou, L. Chen, C. Fu, N. Song, B. Yao, Protein palmitoylation-mediated palmitic acid sensing causes blood-testis barrier damage via inducing ER stress. *Redox Biol.* **54**, 102380 (2022).
51. X. Ren, X. Yang, B. Cheng, X. Chen, T. Zhang, Q. He, B. Li, Y. Li, X. Tang, X. Wen, Q. Zhong, T. Kang, M. Zeng, N. Liu, J. Ma, HOPX hypermethylation promotes metastasis via activating *SNAIL* transcription in nasopharyngeal carcinoma. *Nat. Commun.* **8**, 14053 (2017).

Acknowledgments: We would like to thank B. Yao (Jinling Hospital, Nanjing University, School of Medicine) and J. Cui (School of Life Sciences, Sun Yat-sen University) for technical assistance with the protein palmitoylation experiments, and J.X. Feng and S. Gao for technical assistance with the gel filtration chromatography experiment. **Funding:** This work was supported by grants from the National Natural Science Foundation of China (81802707 and 82172749 to Y.-P.C., 82203049 to J.-W.L., and 82102875 to Y.-Q.W.), the National Key R&D Program of China (2021YFA0909800 to Y.-P.C.), the Natural Science Foundation of Guangdong Province (2021B1515020010 to Y.-P.C.), the National Postdoctoral Program for Innovative Talents (BX2021386 to J.-W.L.), and the Fundamental Research Funds for the Central Universities, Sun Yat-sen University (22yqkq14 to Y.-P.C.). Y.-P.C. also received support from the Sun Yat-sen University Cancer Center Promotion Program for Talented Youth of the National Natural Science Foundation of China. **Author contributions:** Y.-Q.W., J.-W.L., and Y.-P.C. conceived the ideas and wrote the manuscript. Z.-W.H., Y.-P.C., and J.-W.L. contributed to the bioinformatic analysis. Y.-Q.W., D.-H.W., and J.-Y.S. conducted the experiments under the supervision of D.W., X.-Y.L., J.L., and Y.-P.C. Y.-Q.W., J.-W.L., and Y.-P.C. analyzed data and produced figures. D.W., X.-Y.L., W.C.S.C., and J.M. provided technical assistance. Y.-Q.W., D.W., D.-H.W., X.-Y.L., W.C.S.C., J.-W.L., and Y.-P.C. contributed to manuscript revision. J.-W.L. and Y.-P.C. supervised the project. All authors approved the manuscript. **Competing interests:** The authors declare that they have no competing interests. **Data and materials availability:** All data needed to evaluate the conclusions in the paper are present in the paper and/or the Supplementary Materials. The microarray data used in this study were obtained from the Gene Expression Omnibus (GEO; www.ncbi.nlm.nih.gov/geo/) under accession number GSE12452, while the bulk RNA-seq and scRNA-seq data were under accession numbers GSE102349 and GSE150430, respectively. ChIP-seq data for BZW2 were obtained from the GEO under the accession number GSE174559. The authenticity of this manuscript was validated by uploading the key raw data to the Research Data Deposit public platform (RDDDB2022814506) (www.researchdata.org.cn). The R script code is available at Zenodo (DOI: 10.5281/zenodo.7194412).

Submitted 22 May 2022
Accepted 6 December 2022
Published 6 January 2023
10.1126/sciadv.add0960